NASA Technical Paper 1120

Numerical Study of Transonic Flow Over Oscillating Airfoils Using the Full Potential Equation

Koji Isogai

APRIL 1978

NASA

NASA Technical Paper 1120

Numerical Study of Transonic Flow Over Oscillating Airfoils Using the Full Potential Equation

Koji Isogai
Langley Research Center
Hampton, Virginia

National Aeronautics
and Space Administration

**Scientific and Technical
Information Office**

1978

SUMMARY

The behavior of unsteady aerodynamic loadings on airfoils oscillating in transonic flow has been investigated numerically with particular attention given to supercritical airfoil sections. A previously developed finite difference method, which is based on the full potential equation and which uses a quasi-conservative scheme for proper capture of shock wave motion, was employed for the present study. The unsteady aerodynamic pressure and load distributions on several different airfoil sections are presented with particular emphasis on the effects of free-stream Mach number, reduced frequency, and mean angle of attack. These parameters are demonstrated to have a significant effect on the behavior of the unsteady aerodynamic loadings. Comparisons of the present calculations with the exact inviscid solution and with the experimental results are also presented.

INTRODUCTION

Recent development of supercritical airfoil sections has led to improvements in aerodynamic efficiency at high subsonic speeds. This situation has stimulated considerable interest in unsteady aerodynamics of supercritical airfoil sections (refs. 1 and 2). This interest was reinforced when wind-tunnel tests (ref. 3) showed that a supercritical wing experiences a more pronounced dip of the flutter boundary in the transonic regime in comparison to a structurally similar conventional wing.

Recently, reference 4 presented a method for solving the full potential equation by a time marching finite difference technique. The method was a quasi-conservative scheme to capture shock wave motion properly. The capability of the method for treating a supercritical airfoil section was well demonstrated by numerical examples in reference 4. No systematic investigation of the behavior of unsteady aerodynamic loadings was attempted, however. Since the supercritical transonic flow field (especially about supercritical airfoil sections) is sensitive to changes of free-stream Mach number and angle of attack, a considerable effect of these parameters on the behavior of unsteady aerodynamic loadings is expected. In this paper, the method of reference 4 is applied in an investigation of the behavior of unsteady aerodynamic loadings on oscillating airfoils (including supercritical airfoils). Particular emphasis is given to the effects of mean angle of attack, free-stream Mach number, reduced frequency, and airfoil shape.

The items investigated in the present paper can be summarized as follows:

(a) Behavior of unsteady aerodynamic loadings on supercritical airfoils at design and off-design conditions.

(b) Comparison of unsteady aerodynamic forces, pitching moments, and load distributions between a supercritical airfoil and a conventional airfoil.

(c) Effect of mean angle of attack on unsteady load distributions on a supercritical airfoil.

(d) Behavior of higher harmonics of unsteady aerodynamic loadings.

SYMBOLS

A_n, B_n — harmonic component of total lift coefficient or pitching-moment coefficient ($n = 0, 1, \ldots, N$)

a_n, b_n — harmonic component of pressure loading coefficient ($n = 0, 1, \ldots, N$)

b — semichord

C_L — lift coefficient

C_{L_θ} — first harmonic of lift coefficient per unit θ

C_m — pitching-moment coefficient taken about midchord (positive nose up)

C_{m_θ} — first harmonic of pitching-moment coefficient per unit θ

C_p — pressure coefficient, $\dfrac{p - p_\infty}{\frac{1}{2}\rho_\infty V_\infty^2}$

C_p^* — pressure coefficient at sonic condition

ΔC_p — pressure loading coefficient $\left(\Delta C_p = C_p^L - C_p^U\right)$

$\Delta C_{p,\theta}'$, $\Delta C_{p,\delta}'$ — in-phase component of the first harmonics of the pressure loading coefficient per unit θ and δ, respectively

$\Delta C_{p,\theta}''$, $\Delta C_{p,\delta}''$ — out-of-phase component of the first harmonics of the pressure loading coefficient per unit θ and δ, respectively

i — $= \sqrt{-1}$

k	reduced frequency, $b\omega/V_\infty$
L	lift
M	Mach number
N	highest harmonic
n	nth harmonic (1, 2, 3, . . ., N)
p	pressure
T	time, seconds
t	dimensionless time, $(V_\infty/b)T$
V	total velocity
x	coordinate in chordwise direction normalized by b and measured from midchord
α	angle of attack
α_m	mean angle of attack
δ	angle of control surface (flap) deflection
θ	amplitude of pitching oscillation, radians
ρ	density
ϕ_L, ϕ_m	phase angle between total lift and pitching moment, respectively, and displacement in pitching oscillation, positive for total lift or pitching-moment leading displacement
ω	circular frequency
$\lvert\ \rvert$	magnitude

Subscripts:

t	stagnation condition
∞	free-stream condition

Superscripts:

U,L	upper and lower surface of airfoil

RESULTS FOR A NACA 64A006 AIRFOIL WITH AN OSCILLATING FLAP

Comparisons between the present full potential calculation and the inviscid results obtained by using the Euler equations in reference 5 (Magnus and Yoshihara) are presented in this section. The case considered is a NACA 64A006 airfoil with oscillating quarter-chord flap at $M_\infty = 0.875$ and $k = 0.234$. Comparisons of the steady pressure distributions for the two calculations are shown in figure 1. For reference, experimental results from reference 6 (Tijdeman and Schippers) are also shown. The agreement between the present full potential calculation and the exact inviscid result is satisfactory. The discrepancy between experiment and calculations can possibly be attributed to the wind-tunnel wall interference and boundary-layer effects as discussed in reference 7.

Comparisons of unsteady pressure distributions between the two calculations are shown in figures 2(a) to 2(d) for upper and lower surface pressures at two different phases of the oscillation of the quarter-chord flap. Although the present full potential calculation predicts a slightly stronger shock wave than that of the exact result, the overall agreement between the two calculations is good. The prediction of the stronger shock wave by the present method is reasonable because the shock jump relation of the full potential equation gives a stronger shock wave than that of the Rankine-Hugoniot shock jump relation (ref. 8). The same degree of agreement between the two calculations was obtained for other phases of the flap oscillation.

In-phase and out-of-phase components of the unsteady load distributions for the same case are compared with experimental results obtained from reference 6 in figures 3(a) and 3(b). Although qualitative agreement between the calculation and experiment is good, there is some quantitative discrepancy. Reference 7 pointed out that the discrepancy between calculations, including the boundary-layer correction and experimental results, can be greatly reduced if the nominal free-stream Mach number of the experiment (0.875) is reduced to 0.850 to allow for the wind-tunnel wall interference.

Although the present computer code is not capable of treating the boundary-layer effect, the discrepancy between the calculation and experiment in figures 3(a) and 3(b) can be reduced by adjusting the free-stream Mach number (of the calculation) so that the theoretical shock position of the mean steady flow comes as close as possible to the experimental shock position obtained at $M_\infty = 0.875$. The closest agreement of the steady shock position between the theory and experiment is obtained at $M_\infty = 0.860$ rather than at $M_\infty = 0.850$ obtained in reference 7, as shown in figure 4. The corresponding unsteady results are compared with the experimental results from reference 6 in figures 5(a) and 5(b). The agreement between the two results is markedly improved. This result indicates that the mismatch of the shock position between the calculation and experiment is the predominant factor in the disagreement of the load distribution between the theory and experiment shown in figures 3(a) and 3(b).

RESULTS FOR A SUPERCRITICAL AIRFOIL OSCILLATING IN PITCH AT DESIGN AND OFF-DESIGN CONDITIONS

Calculations of steady pressure distributions and unsteady load distributions were performed for the 70-10-13 supercritical airfoil of reference 9 for three different flow conditions:

Case 1: $M_\infty = 0.71$, $\alpha_m = 0^\circ$ (off design)

Case 2: $M_\infty = 0.70$, $\alpha_m = 0^\circ$ (design)

Case 3: $M_\infty = 0.68$, $\alpha_m = 1^\circ$ (off design)

The steady pressure distribution for each case is shown in figure 6(a). The calculations for unsteady load distributions corresponding to these steady flow conditions were performed for the airfoil oscillating in pitch about the mid-chord axis with an amplitude of 1° at the reduced frequency of 0.10. The unsteady load distribution (the first harmonic) for each case is shown in figure 6(b). The in-phase and out-of-phase components are shown by the solid line and the dashed line, respectively.

Examination of variation of the instantaneous pressure distributions[1] during the cycle of oscillation for these three cases reveals that the patterns of the unsteady shock wave motion on the upper surface are very different for each case. In case 1, the relatively strong shock wave oscillates around its mean position with relatively small excursion amplitude (about 4 percent of the chord) during the cycle of the oscillation. In case 2, a relatively weak shock wave appears and disappears during the cycle of the oscillation in the neighborhood of the part of the airfoil where the local supersonic region of the mean steady flow terminates. In case 3, as discussed later in detail, the relatively weak shock wave on the upper surface oscillates back and forth with large excursion amplitude over the forward part of the airfoil during the cycle of the oscillation.

In figure 6(b), the differences in the unsteady shock wave motion between these three cases are clearly reflected in the unsteady load distributions. In case 1, the relatively strong shock wave causes a peak value near the three-quarter-chord point for both the in-phase and out-of-phase components whereas such a peak value caused by the shock wave is not observed in the load distribution for case 2. In case 3, a bulge appears in the pressure distribution on the front part of the airfoil. Comparison of the full potential unsteady load distribution for case 3 with that of flat-plate theory (see fig. 7) indicates that this bulge contributes considerably to the unsteady total lift and pitching-moment derivatives. Examination of the variation of instantaneous pressure distributions during a cycle of oscillation, shown in figures 8(a) to 8(d), reveals that the formation of this bulge is closely associated with a shock wave on the upper surface which oscillates back and forth with relatively large excursion amplitude. The formation of such a bulge in the unsteady (upper surface) pres-

[1]The instantaneous pressure distributions are shown in this paper only for case 3 (see fig. 8).

sure distribution was also observed experimentally in reference 2 on a NLR 7301 "shock free" airfoil oscillating in pitch at the design condition.

COMPARISON OF RESULTS FOR SUPERCRITICAL AND CONVENTIONAL AIRFOILS OSCILLATING IN PITCH

According to the recent experimental study of reference 3, a wing with a supercritical airfoil experienced a more pronounced dip of a flutter boundary than a structurally similar conventional wing. Unsteady aerodynamic forces are clearly responsible for this phenomenon. Therefore, the difference of the unsteady aerodynamic derivatives and aerodynamic loadings between the two airfoils was investigated. For this purpose a 79-03-12 supercritical airfoil (ref. 9, Bauer et al.) and a NACA 0012 conventional airfoil were selected. Both airfoils have the same ratio of thickness to chord. In figure 9, the steady pressure distribution calculated on the 79-03-12 airfoil for the design condition of $M_\infty = 0.79$ and $\alpha = 0^\circ$ is compared with the design pressure distribution from reference 9. The agreement between the present calculation and the design pressure distribution is satisfactory. In figure 10, the steady pressure distributions of each airfoil at three different free-stream Mach numbers for an angle of attack of 0° are shown. The unsteady calculations have also been performed for these three Mach numbers. The airfoils were considered to be oscillating in pitch about the midchord axis with an amplitude of 1° at a reduced frequency of 0.10.

The magnitudes and phase angles of the unsteady lift (first harmonic) and pitching moment (first harmonic) for both airfoils are shown in figures 11(a) and 11(b), respectively. With the exception of the $M_\infty = 0.75$ case, the mean angle of attack was 0° for all calculations. At $M_\infty = 0.75$, results were also computed for an angle of attack of 1° to illustrate the effect of the mean angle of attack. The values predicted by the flat-plate theory are also presented in the same figures for comparison. The unsteady load distributions (in-phase and out-of-phase components of the first harmonic), which correspond with the steady flows shown in figure 10, are compared in figures 12(a) to 12(c) at each Mach number. For the unsteady lift (see fig. 11(a)), the difference between the two airfoils is surprisingly small. However, this apparent agreement of the total lifts is rather fortuitous. As shown in figures 12(a) to 12(c), there is a considerable difference in the load distribution between the two airfoils except those of $M_\infty = 0.70$ for which the flows are almost subcritical. This dissimilarity in the load distribution between the two airfoils is reflected by the difference in pitching moment (about midchord axis), which becomes greater as the Mach number is increased as shown in figure 11(b). It is also observed in figures 11(a) and 11(b) that the change of the mean angle of attack affects the unsteady lift and moment differently between the two airfoils. In figure 12(c) there is still a considerable nonlinear thickness effect on total lift and pitching moment at $M_\infty = 0.70$ even though the flow is almost subcritical. This effect can be confirmed by comparing load distributions for the nonlinear results with flat-plate theory.

RESULTS FOR EFFECT OF MEAN ANGLE OF ATTACK FOR A SUPERCRITICAL AIRFOIL OSCILLATING IN PITCH

Mean angle of attack was shown to affect both the unsteady total lift and pitching moment for the 79-03-12 and NACA 0012 airfoils (figs. 11(a) and 11(b)). Angle-of-attack effects are, therefore, examined more closely for the 79-03-12 airfoil. In figure 13, steady pressure distributions for the 79-03-12 supercritical airfoil at $M_\infty = 0.75$ at two different angles of attack (0° and 1°) are shown. At $\alpha = 0^\circ$, the steady flow is slightly supercritical near the leading-edge region without shock wave, whereas at $\alpha = 1^\circ$ the local supersonic region on the upper surface is increased, being terminated with a weak shock wave near the 40-percent-chord point.

For unsteady calculations the airfoil is oscillated in pitch with an amplitude of 1° at $k = 0.10$ about these different mean angles of attack (0° and 1°). The in-phase and out-of-phase components (the first harmonic) of the unsteady load distributions corresponding to these two different mean angles of attack are compared in figure 14. The mean angle of attack has a striking effect. Such a difference in the load distribution comes from the difference of the unsteady shock wave pattern in the two cases. For the case of $\alpha_m = 0^\circ$, the shock wave does not appear during the cycle of oscillation, whereas for the case of $\alpha = 1^\circ$, the relatively weak shock wave oscillates back and forth over the forward portion of the upper surface of the airfoil. This behavior is evident in the variation of the instantaneous pressure distribution shown in figure 15.

RESULTS FOR HIGHER HARMONICS OF LOADING ON AIRFOILS OSCILLATING IN PITCH

In transonic flow, effects of the shock wave displacement cause nonsinusoidal variations in the local pressures on some parts of the airfoil. In this section, the chordwise distributions of higher harmonic components of unsteady aerodynamic loadings on two different airfoils which exhibit different unsteady shock wave pattern, are examined. The first case considered is the 79-03-12 supercritical airfoil oscillating in pitch about the midchord axis at $M_\infty = 0.75$ and $k = 0.10$. The mean angle of attack and the amplitude of the oscillation are both 1°. The steady pressure distribution for this case is shown in figure 13(b). The instantaneous pressures for the oscillating case are shown in figures 15(a) to 15(d). The relatively weak shock wave oscillates around the 40-percent-chord point with relatively large shock excursion amplitude (about 25-percent chord). The shock wave changes its strength considerably during the cycle of oscillation (the shock wave disappears at its maximum upstream position as seen in fig. 15(d)).

Harmonic analysis of the time-varying load distributions was made. The resulting coefficients of the harmonics are used to define ΔC_p in the following equation:

$$\Delta C_p = a_0 + \theta \sum_{n=1}^{N} \left[a_n \cos (nkt) + b_n \sin (nkt) \right]$$

The chordwise distributions of b_n (n = 1, 2, 3) and a_n (n = 1, 2, 3) are plotted in figures 16(a) and 16(b), respectively. In these figures, two characteristics of the higher harmonics (n = 2, 3) are evident. First, the region where the magnitudes of the higher harmonics are appreciable is confined to the portion of the airfoil over which the shock wave oscillates back and forth (see figs. 15(a) to 15(d)). Second, the higher harmonics exhibit a wavy pattern in the chordwise direction. As the simplified model used in reference 2 shows, the existence of the wavy pattern of the higher harmonics is the natural consequence of the excursion of the sharp pressure rise associated with the moving shock wave.

To determine the effect of reduced frequency on harmonics of the load distributions, the unsteady calculation for $k = 0.30$ was also performed without changing the other flow conditions. The results are shown in figures 17(a) and 17(b). Some effect of the reduced frequency is observed on both the first harmonic and higher harmonics. The region where the higher harmonics are relatively large is decreased for the higher reduced frequency. This result is caused by a reduction in shock excursion amplitude at the higher reduced frequency.

The second case considered is that of a NACA 0012 airfoil oscillating in pitch about midchord axis at $M_\infty = 0.79$ and $k = 0.10$. The steady pressure distribution and the variation of the instantaneous pressure distribution are shown in figure 18 and figures 19(a) to 19(d), respectively. The relatively strong shock wave oscillates about the midchord position with a relatively small excursion amplitude (about 12-percent chord). The chordwise distributions of harmonic components b_n (n = 1, 2, 3) and a_n (n = 1, 2, 3) of the loading are shown in figures 20(a) and 20(b), respectively. Again, the region where the higher harmonics are appreciable is confined to the part of the airfoil over which the shock wave excursion occurs. The higher harmonics differ from the previous case because the magnitude of the second and third harmonics (b_2, b_3, a_2, and a_3) is relatively small in comparison with the very large peak values of the first harmonics (b_1 and a_1) observed in the region near the oscillating shock wave.

As pointed out in reference 2, the contribution of higher harmonic components to the unsteady total lift and pitching moment might be relatively small in comparison with the contribution of the first harmonic because of their wavy chordwise distributions. This result can be confirmed in table I where harmonic components of the total lift and pitching moment for both cases (79-03-12 supercritical airfoil and NACA 0012) are shown. The harmonic components A_n (n = 0, 1, 2, 3) and B_n (n = 1, 2, 3) of the total lift and pitching moment are defined by the following equation:

$$\begin{matrix} C_L \\ \text{or} \\ C_m \end{matrix} = A_0 + \theta \sum_{n=1}^{N} \left[A_n \cos (nkt) + B_n \sin (nkt) \right]$$

The magnitude of the higher harmonic components is less than 8 percent of the first harmonic components for case 1 and less than 2 percent of the first harmonic components for case 2.

CONCLUDING REMARKS

A numerical study has been performed to investigate the behavior of the unsteady aerodynamic forces and moments, load distributions, and pressure distributions on airfoils (including supercritical airfoils) oscillating in a transonic flow. Particular emphasis has been placed on the effect of free-stream Mach number, mean angle of attack, and reduced frequency. It has been shown that these parameters have a significant effect on the behavior of the unsteady aerodynamic loadings. Generally, the change of the parameters produced a different pattern of the unsteady shock wave motion, which played the predominant role in determining the unsteady aerodynamic load distributions.

Since the present results are based on the inviscid flow calculations, the potentially important effect of the boundary layer has been neglected. However, good agreement for the unsteady load distributions between calculation and experiment was obtained by adjusting the free-stream Mach number so that the theoretical and experimental steady shock positions are in agreement. Thus, the inviscid flow appears to play a dominant role in determining the behavior of the unsteady aerodynamic loadings as long as the boundary layer remains attached. Although the inclusion of the boundary-layer effect is obviously necessary, the present results, based on the inviscid flow calculations, give insight into the unsteady transonic aerodynamics of oscillating airfoils.

Langley Research Center
National Aeronautics and Space Administration
Hampton, VA 23665
January 17, 1978

REFERENCES

1. Tijdeman, H.: On the Unsteady Aerodynamic Characteristics of Oscillating Airfoils in Two-Dimensional Transonic Flow. NLR MP 76003 U, Nat. Aero-Astronaut. Res. Inst. (Amsterdam), Mar. 4, 1976.

2. Tijdeman, H.; Schippers, P.; and Persoon, A. J.: Unsteady Airloads on an Oscillating Supercritical Airfoil. Unsteady Airloads in Separated and Transonic Flow, AGARD-CP-226, Apr. 1977, pp. 12-1 - 12-15.

3. Farmer, Moses G.; and Hanson, Perry W.: Comparison of Supercritical and Conventional Wing Flutter Characteristics. AIAA/ASME/SAE 17th Structures, Structural Dynamics, and Materials Conference (King of Prussia, Pennsylvania), May 1976, pp. 608-614.

4. Isogai, Koji: Calculation of Unsteady Transonic Flow Over Oscillating Airfoils Using the Full Potential Equation. AIAA/ASME 18th Structures, Structural Dynamics & Materials Conference, Volume B (San Diego, California), Mar. 1977, pp. 245-256.

5. Magnus, R.; and Yoshihara, H.: The Transonic Oscillating Flap. AIAA Paper No. 76-327, July 1976.

6. Tijdeman, H.; and Schippers, P.: Results of Pressure Measurements on an Airfoil With Oscillating Flap in Two-Dimensional High Subsonic and Transonic Flow (Zero Incidence and Zero Mean Flap Position). NLR TR 73078 U, Nat. Lucht - Ruimtevaartlab. (Amsterdam), July 13, 1973.

7. Magnus, R.; and Yoshihara, H.: The Transonic Oscillating Flap - A Comparison of Calculations With Experiments. Unsteady Airloads in Separated and Transonic Flow, AGARD-CP-226, Apr. 1977, pp. 13-1 - 13-5.

8. Van der Vooren, J.; and Slooff, J. W.: Difference in Inviscid Isentropic Models Used for Finite Difference Calculation of Transonic Flow With Shocks About Airfoils; the Prediction of Wave Drag. NLR TR 74002 U, Nat. Aero-Astronaut. Res. Inst. (Amsterdam), Jan. 14, 1974.

9. Bauer, Francis; Garabedian, Paul; Korn, David; and Jameson, Antony: Supercritical Wing Sections II. Volume 108 of Lecture Notes in Economics and Mathematical Systems, Springer-Verlag, 1975.

TABLE I.- HARMONIC COMPONENTS OF UNSTEADY TOTAL LIFT AND PITCHING MOMENT ON OSCILLATING 79-03-12 SUPERCRITICAL AIRFOIL AND NACA 0012 AIRFOIL

(a) 79-03-12 supercritical airfoil; $M_\infty = 0.75$; $k = 0.10$; $\alpha_m = 1^\circ$; $\theta = 1^\circ$

	A_0	A_1	B_1	A_2	B_2	A_3	B_3
C_L	0.4872	-4.0362	5.5908	0.2429	0.0104	-0.0331	0.0135
C_m	.0677	-1.4237	1.1547	.0645	.0915	.0094	.0149

(b) NACA 0012 airfoil; $M_\infty = 0.79$; $k = 0.10$; $\alpha_m = 0^\circ$; $\theta = 1^\circ$

	A_0	A_1	B_1	A_2	B_2	A_3	B_3
C_L	-0.0019	-3.4010	6.5862	0.0066	-0.0399	-0.0099	-0.0262
C_m	-.0002	-.9547	1.1693	.0028	-.0202	.0095	-.0123

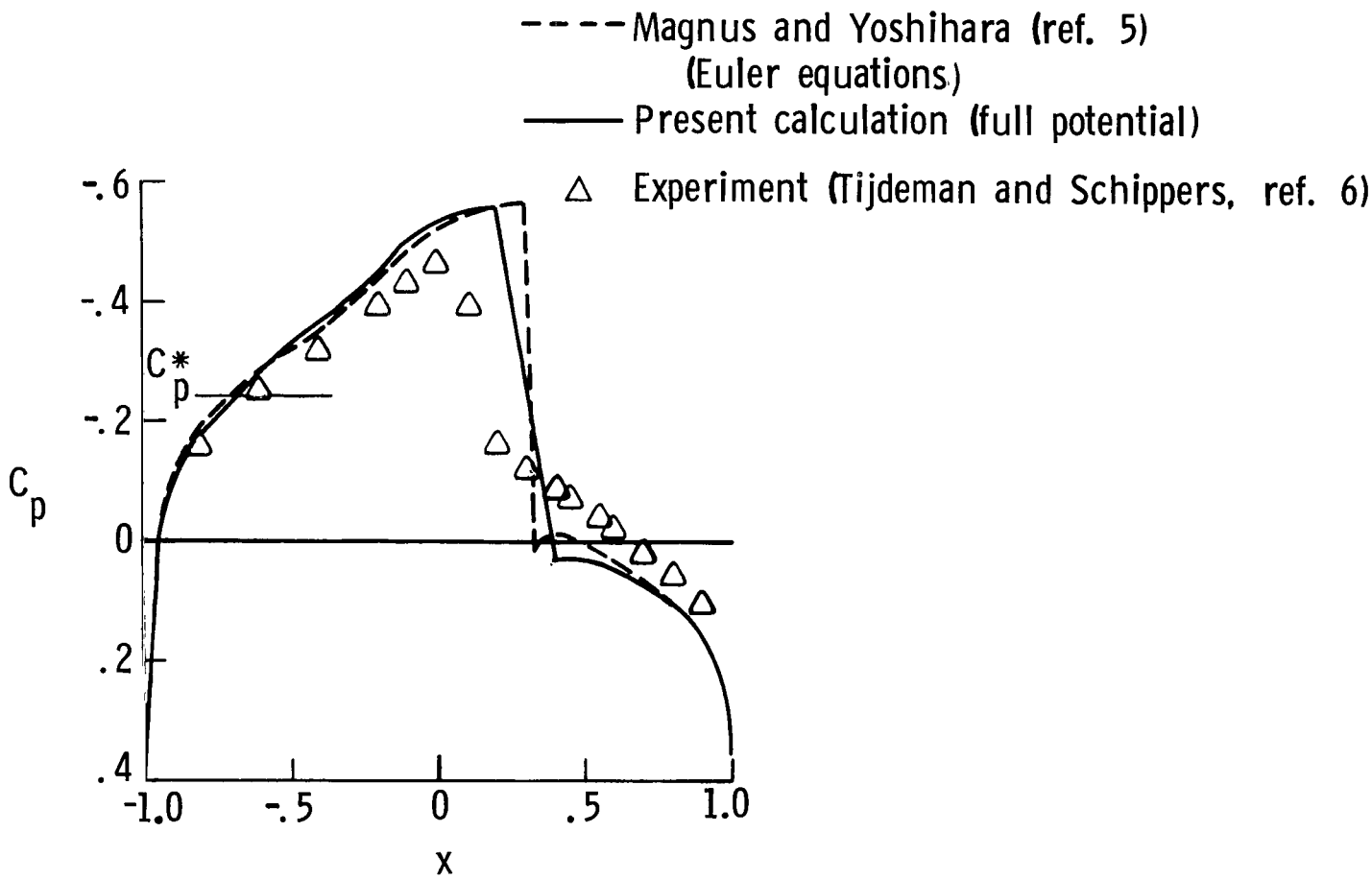

Figure 1.- Steady pressure distributions for NACA 64A006 airfoil.
$M_\infty = 0.875$; $\alpha = 0^\circ$.

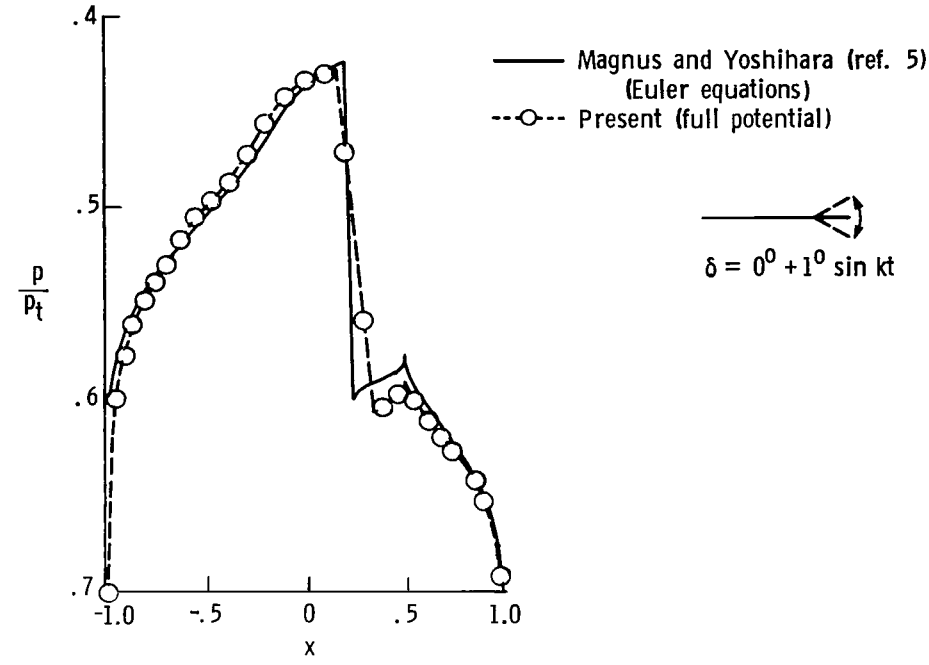

(a) Upper surface; kt = 30°.

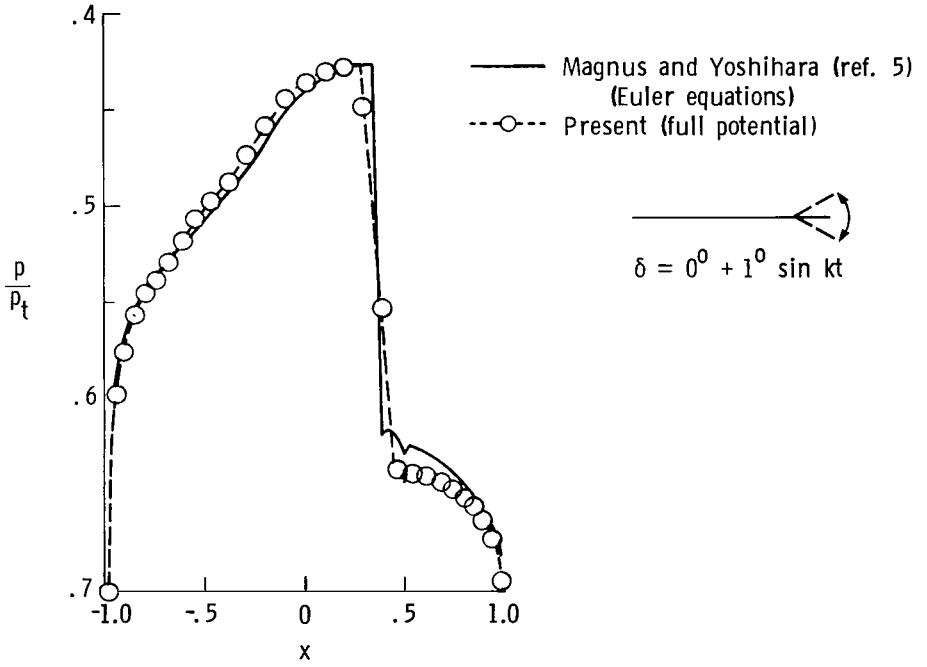

(b) Lower surface; kt = 30°.

Figure 2.- Unsteady pressure distributions on NACA 64A006 airfoil with oscillating quarter-chord flap. M_∞ = 0.875; k = 0.234.

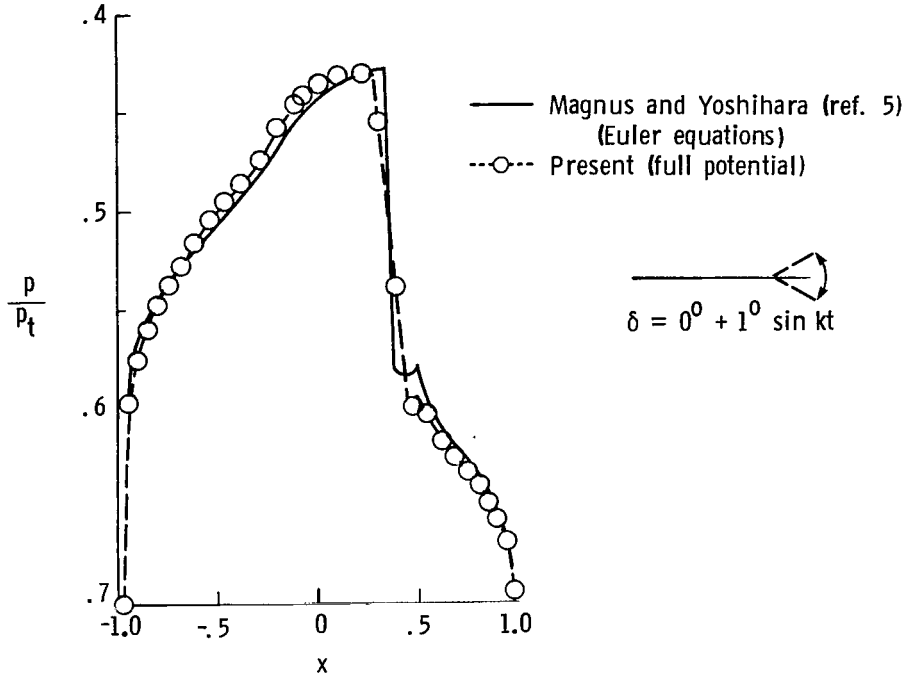

(c) Upper surface; kt = 150°.

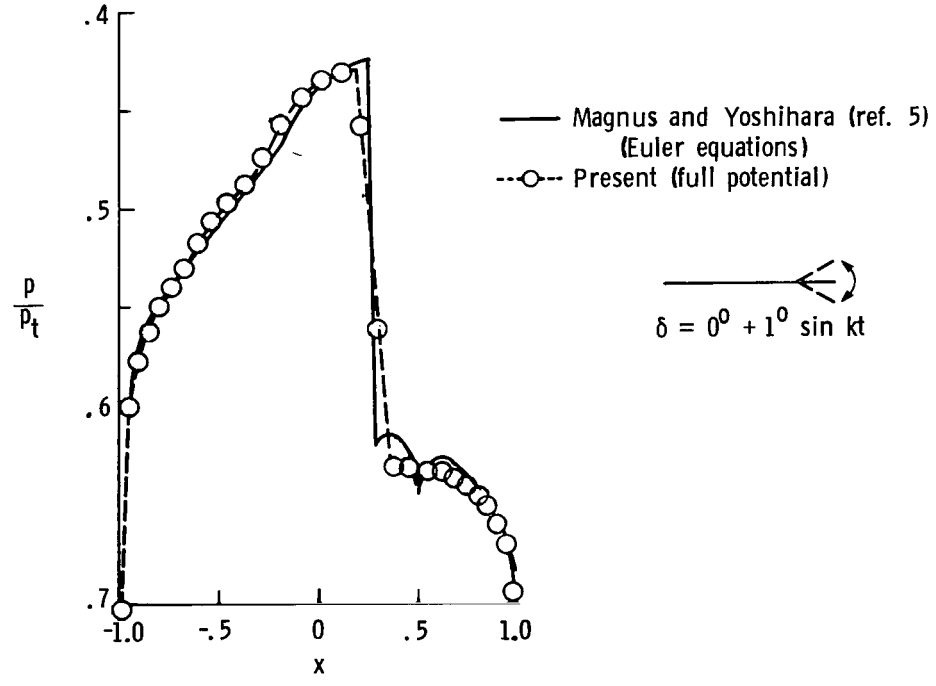

(d) Lower surface; kt = 150°.

Figure 2.- Concluded.

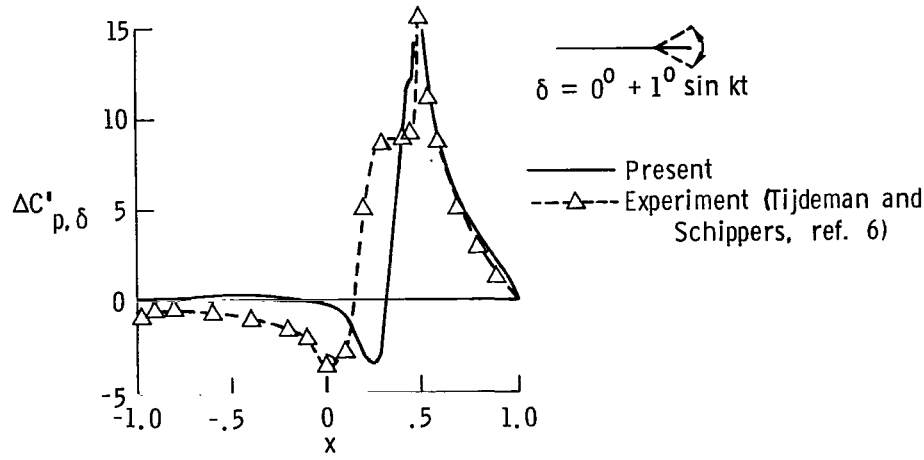

(a) In-phase component.

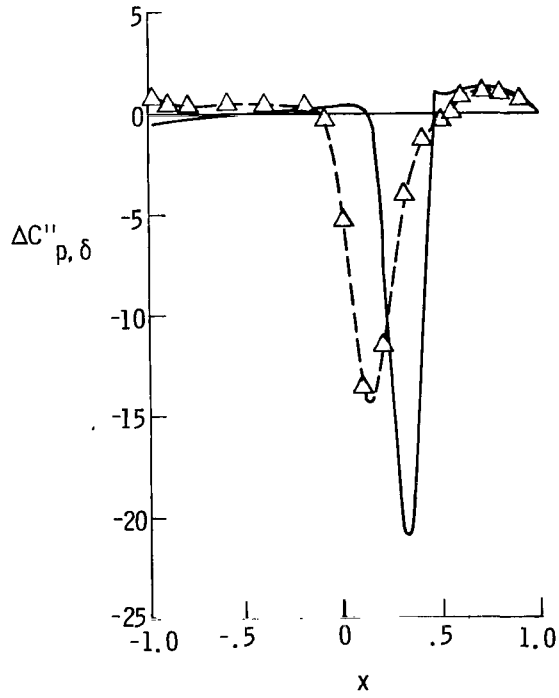

(b) Out-of-phase component.

Figure 3.- Theoretical and experimental unsteady load distributions (first harmonic) on NACA 64A006 airfoil with oscillating flap. $M_\infty = 0.875$; $k = 0.234$.

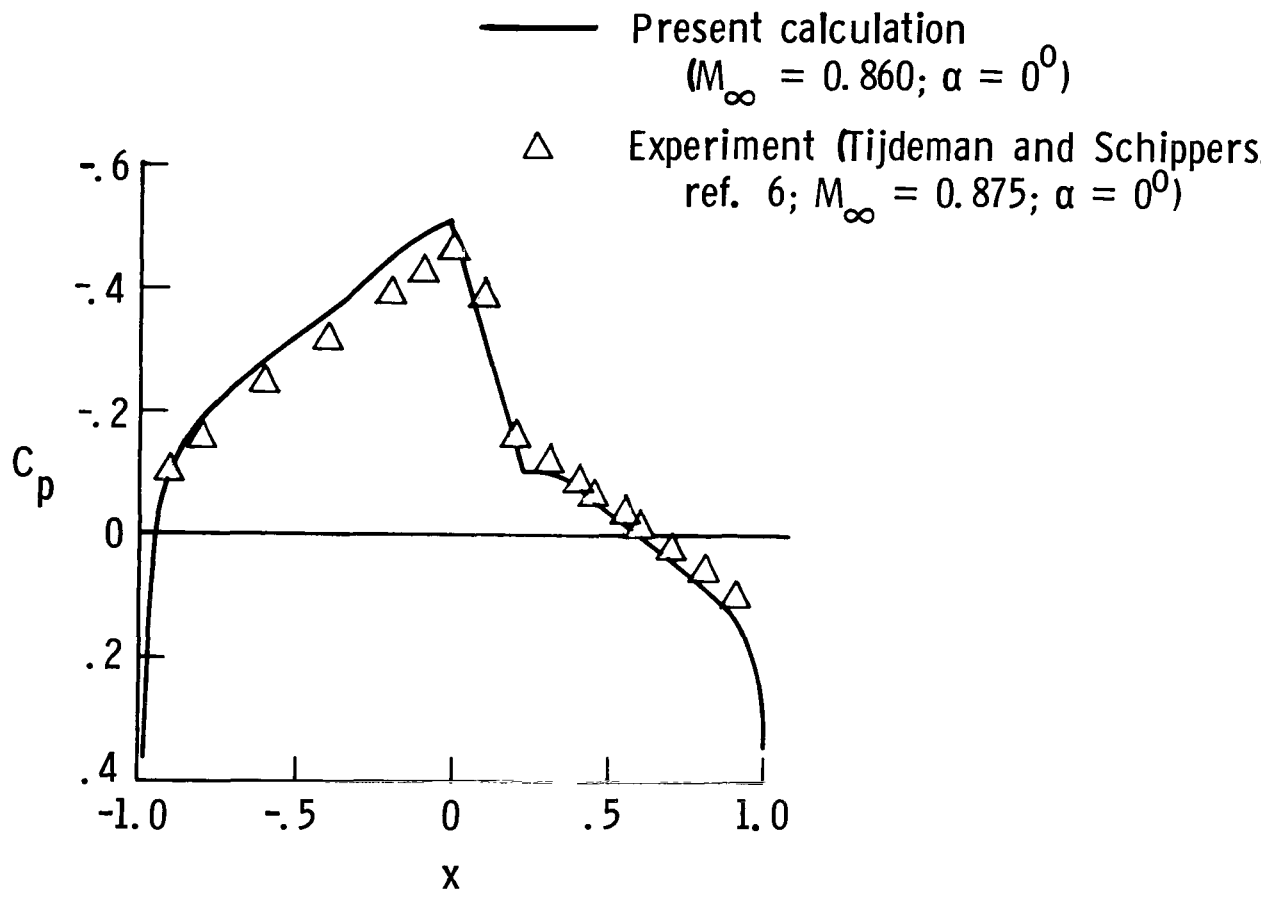

Figure 4.- Theoretical and experimental steady pressure distributions on NACA 64A006 airfoil.

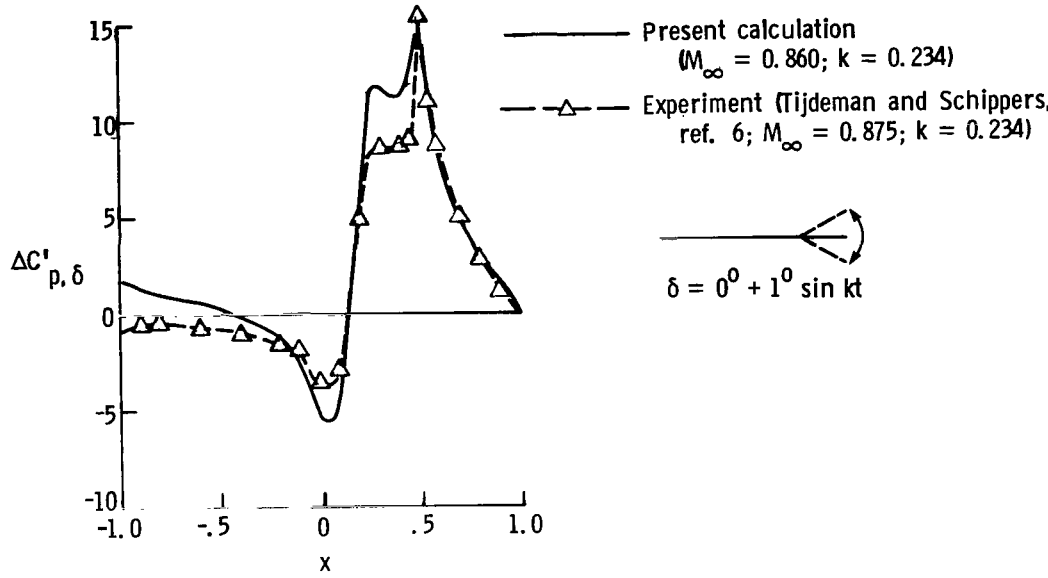

(a) In-phase component.

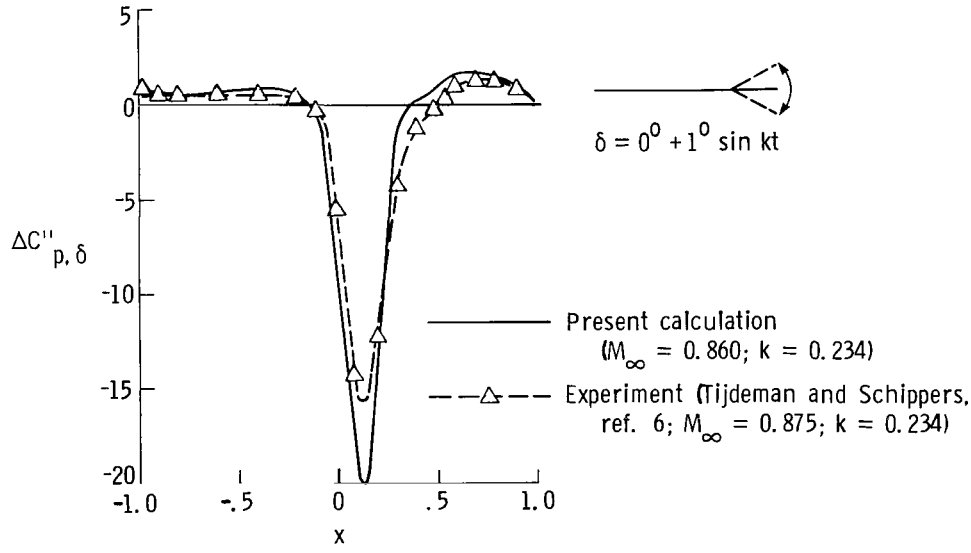

(b) Out-of-phase component.

Figure 5.- Theoretical and experimental unsteady load distributions (first harmonic) on NACA 64A006 airfoil with oscillating flap.

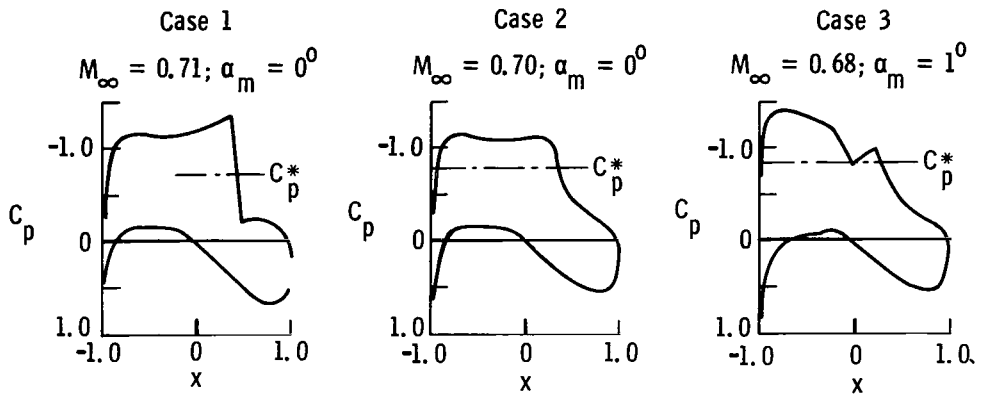

(a) Steady pressure.

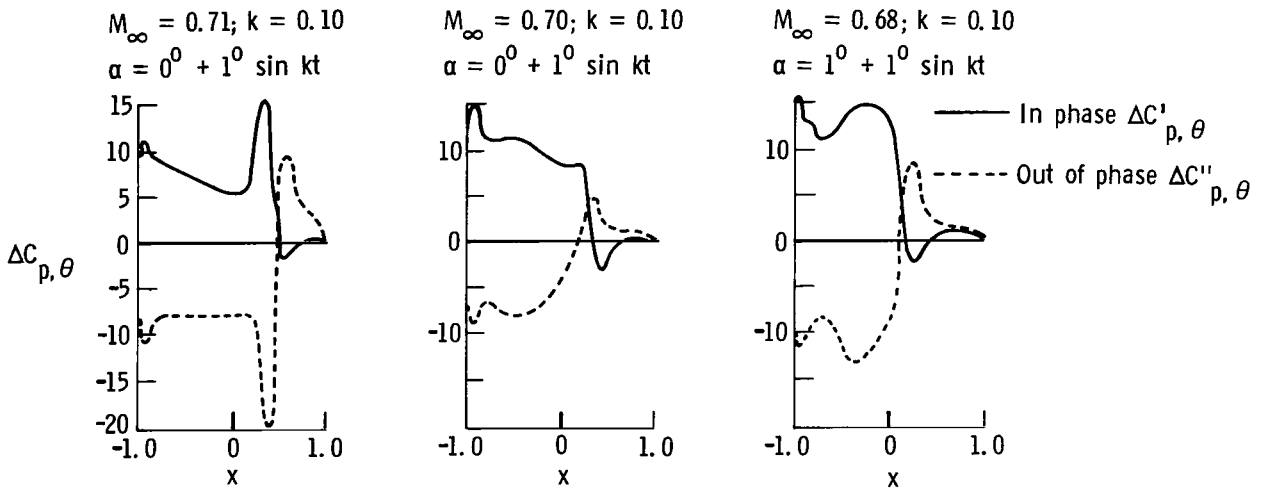

(b) Unsteady load distribution.

Figure 6.- Steady pressure distributions and corresponding unsteady load distributions on 70-10-13 supercritical airfoil oscillating in pitch at design and off-design conditions.

	Flat-plate theory	Full potential
C_{L_θ}	6.17 - 1.45 i	7.39 - 4.52 i
C_{m_θ}	1.51 - 0.629 i	1.58 - 1.49 i

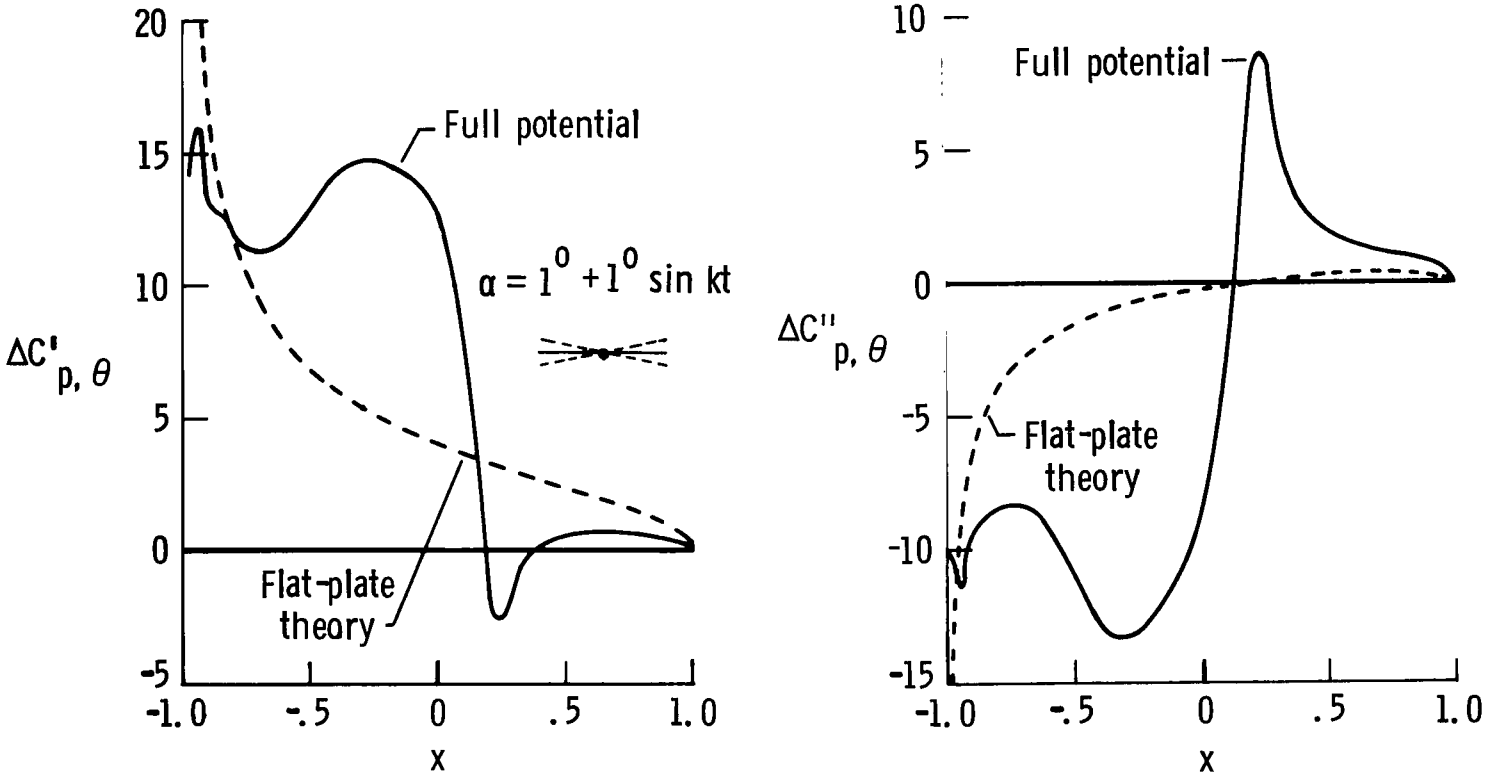

Figure 7.- Calculated unsteady load distributions on 70-10-13 supercritical airfoil oscillating in pitch at off-design conditions. $M_\infty = 0.68$; $k = 0.10$.

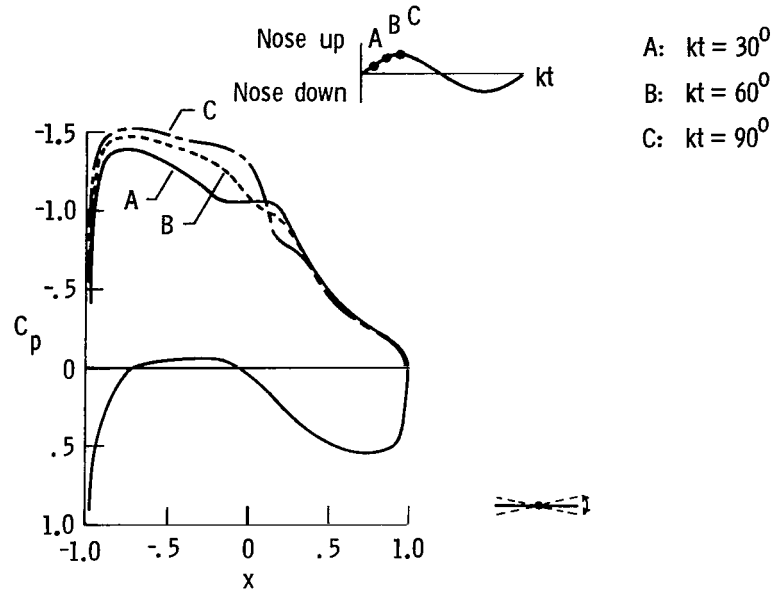

(a) kt = 30°, 60°, 90°.

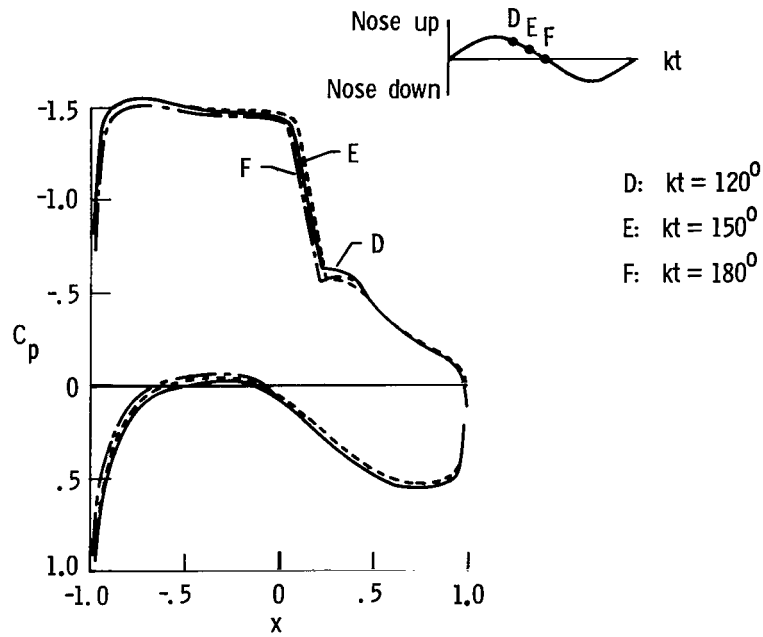

(b) kt = 120°, 150°, 180°.

Figure 8.- Unsteady pressure distribution on 70-10-13 supercritical airfoil oscillating in pitch at off-design condition. M_∞ = 0.68; k = 0.10; α = 1° + 1° sin kt.

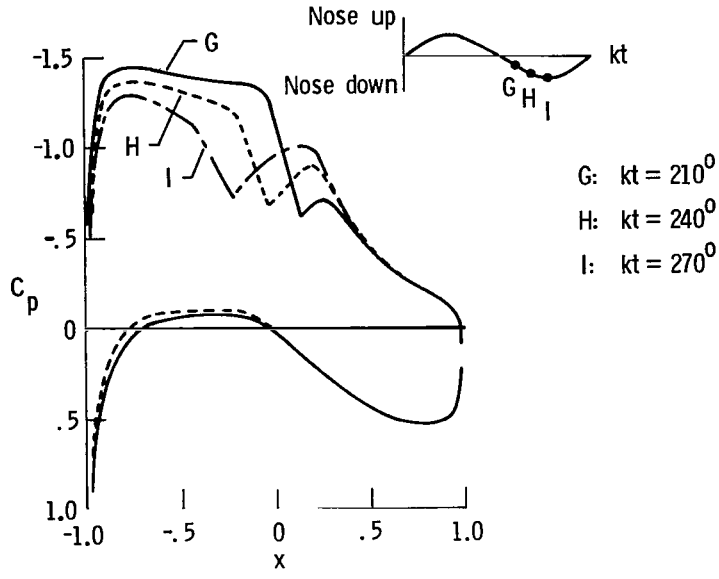

(c) kt = 210°, 240°, 270°.

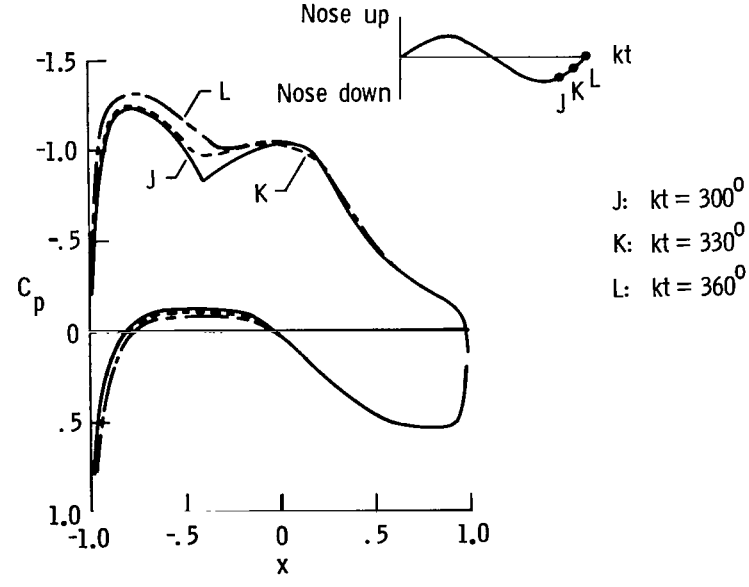

(d) kt = 300°, 330°, 360°.

Figure 8.- Concluded.

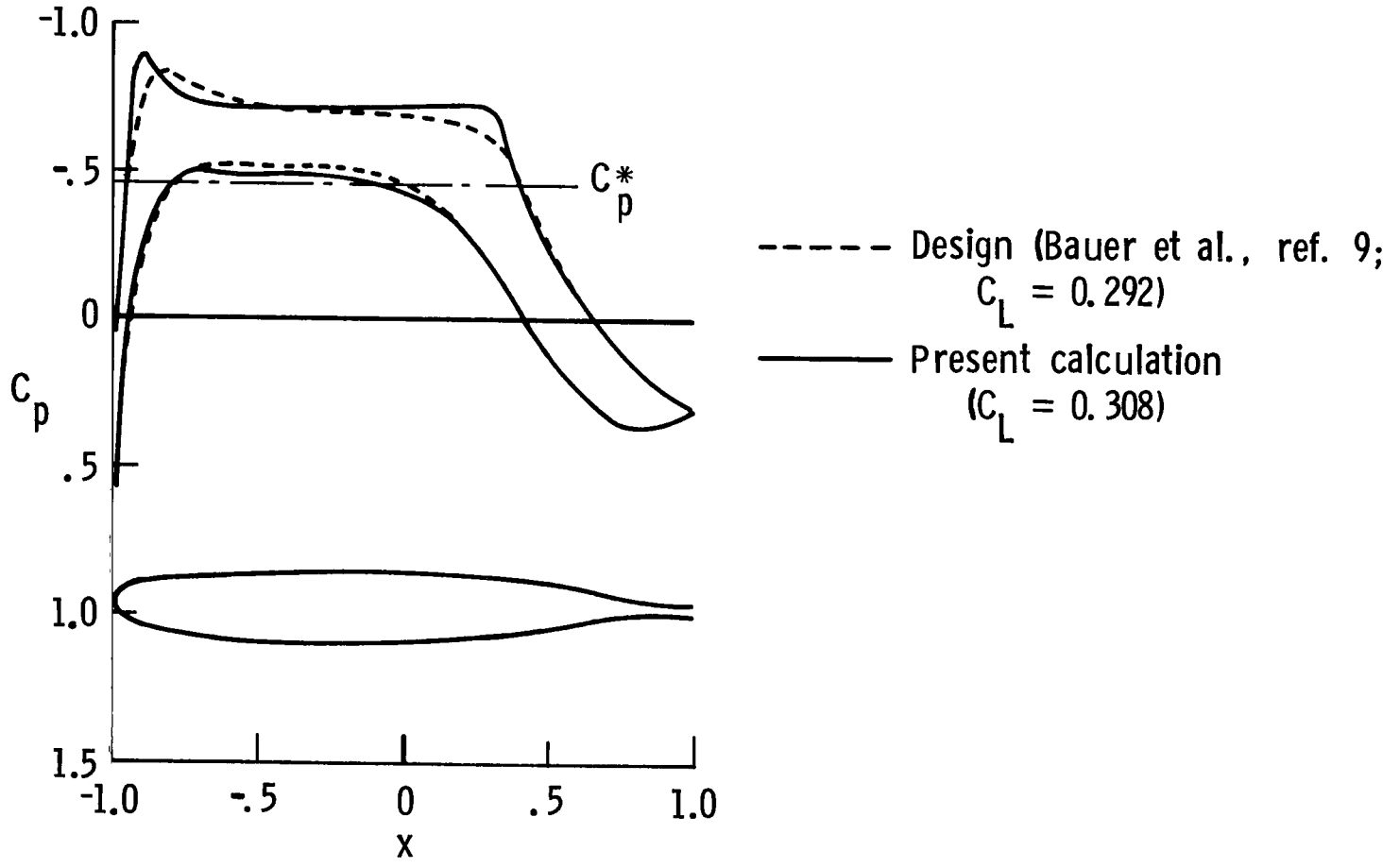

Figure 9.- Steady pressure distribution on 79-03-12 supercritical airfoil in design condition. M_∞ = 0.79; $\alpha = 0^\circ$.

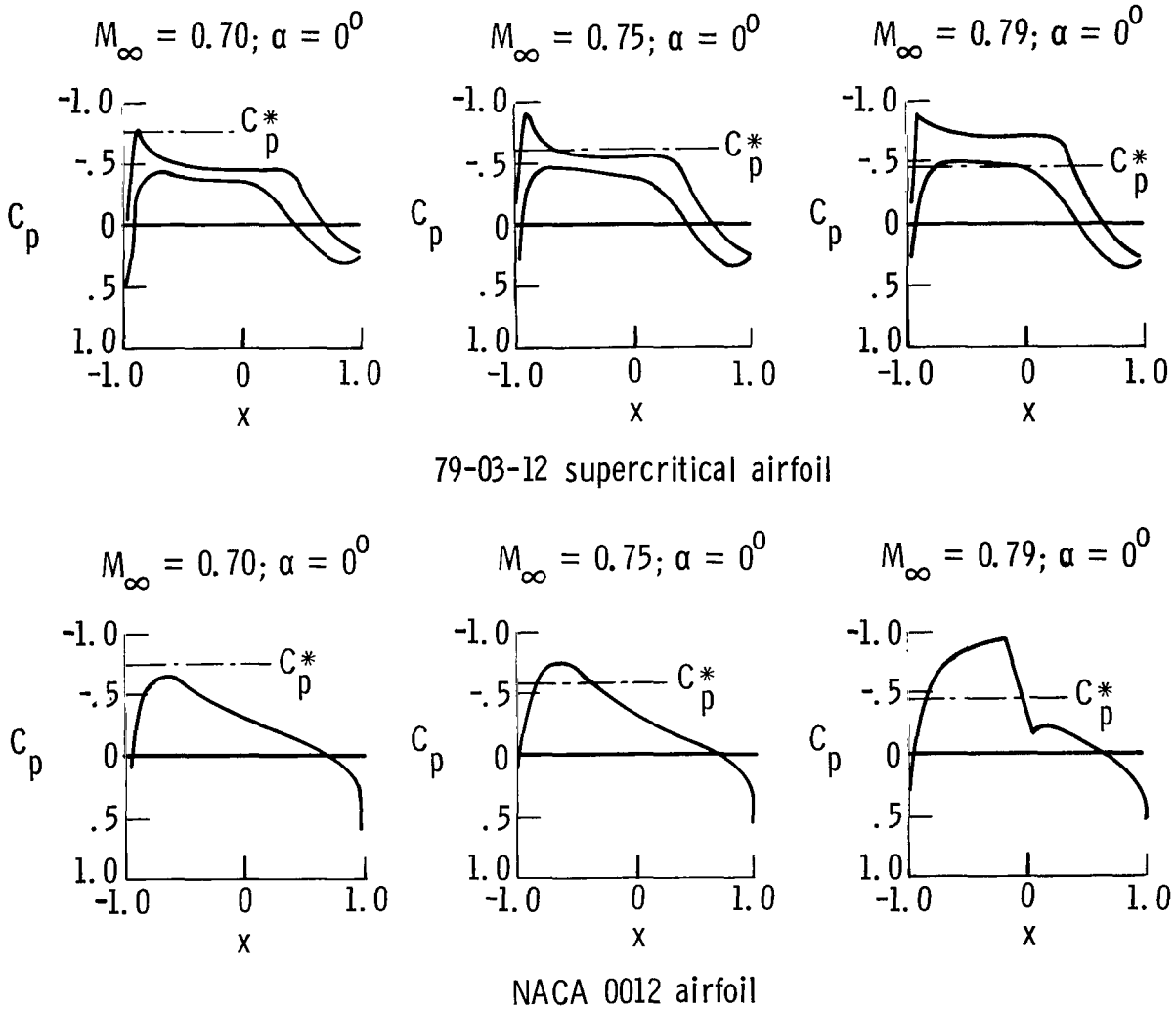

Figure 10.- Steady pressure distributions on 79-03-12 supercritical airfoil and NACA 0012 airfoil.

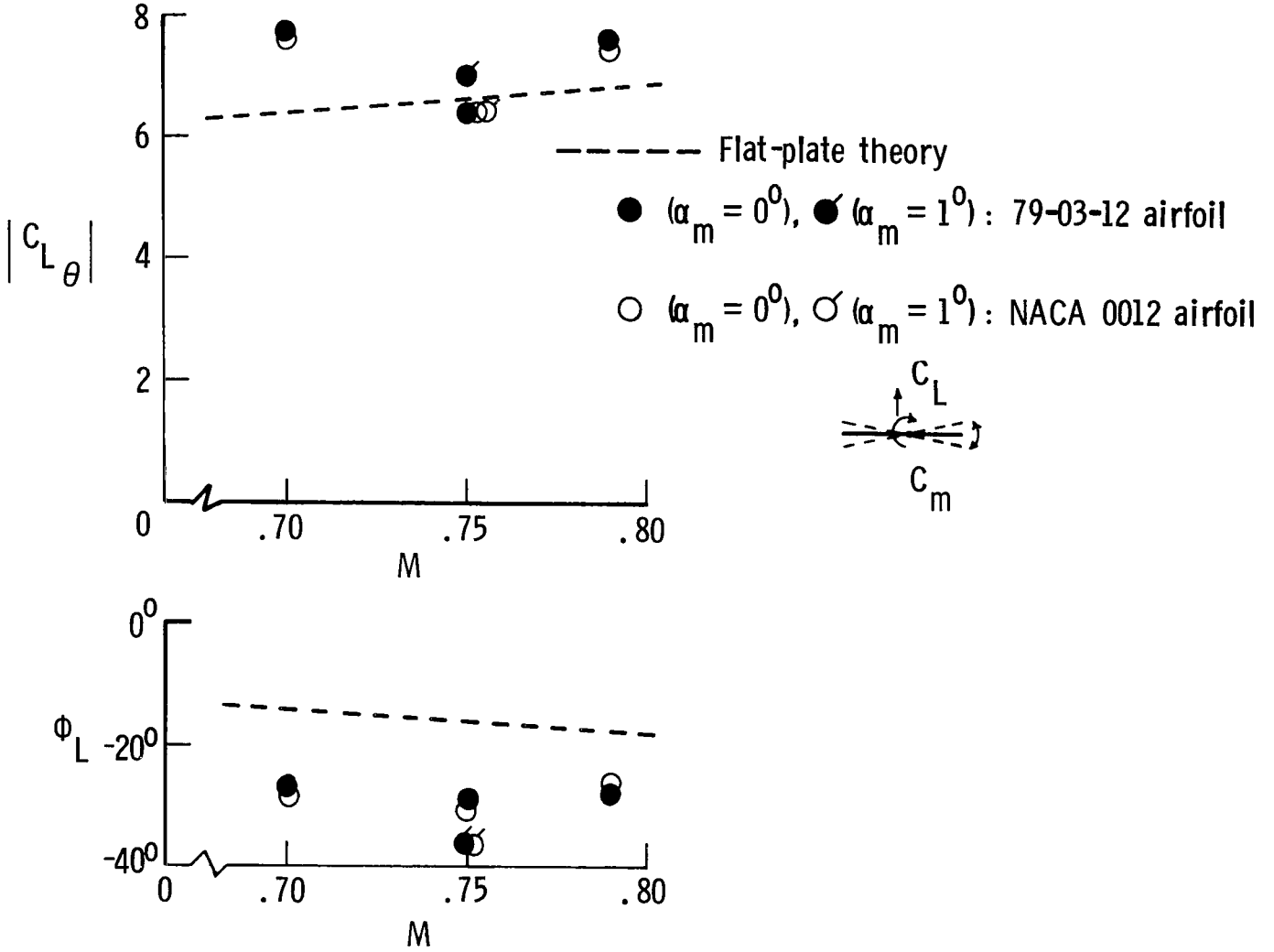

(a) Unsteady lift coefficient.

Figure 11.- Magnitude and phase angle (first harmonic) of lift and pitching moment on oscillating 79-03-12 supercritical airfoil and NACA 0012 airfoil. $k = 0.10$; $\alpha = \alpha_m + 1^o \sin kt$.

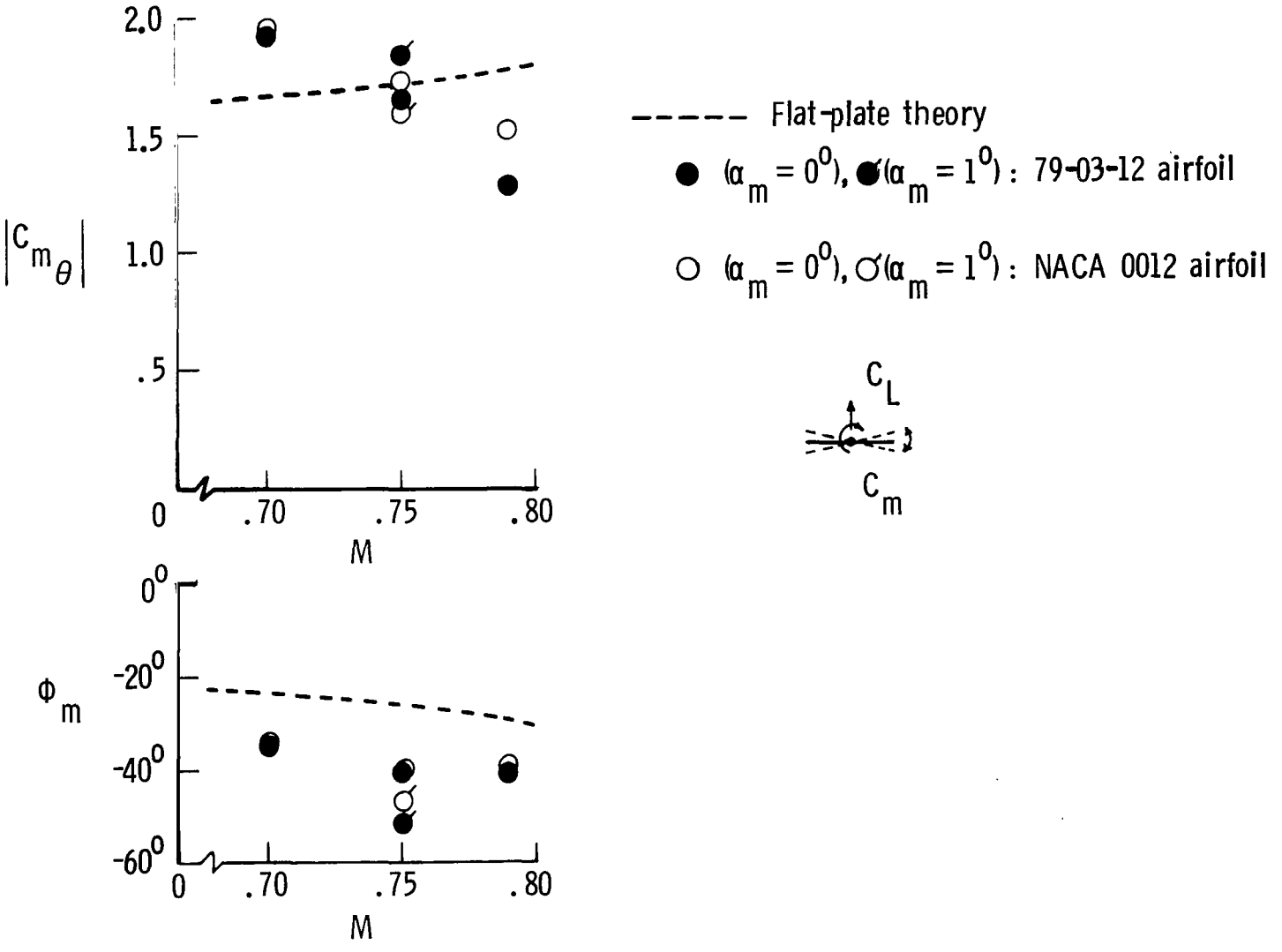

(b) Unsteady pitching-moment coefficient.

Figure 11.- Concluded.

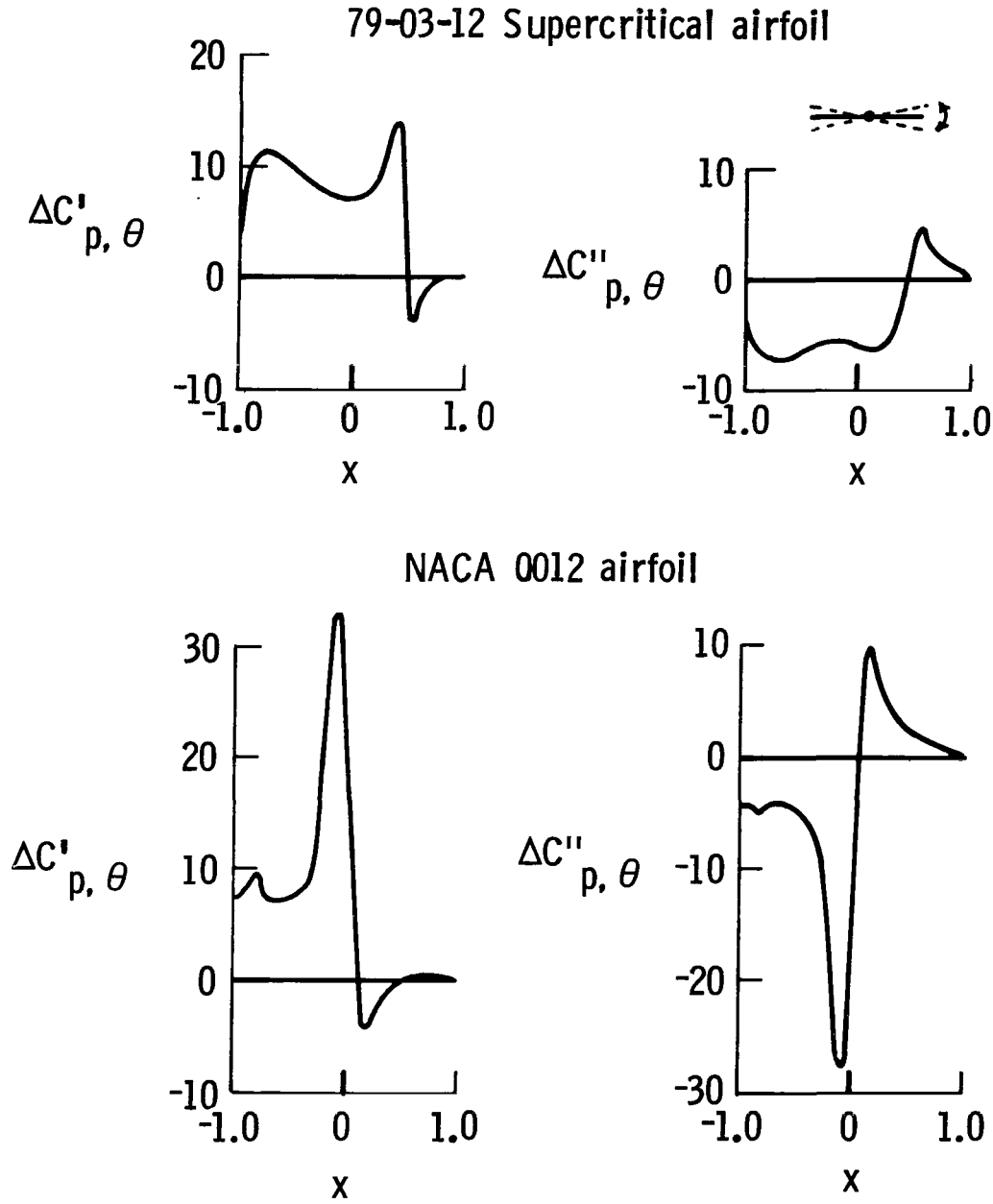

(a) $M_\infty = 0.79$; $k = 0.10$.

Figure 12.- Comparison of unsteady load distributions on 79-03-12 supercritical airfoil and NACA 0012 airfoil. $\alpha = 0^\circ + 1^\circ \sin kt$.

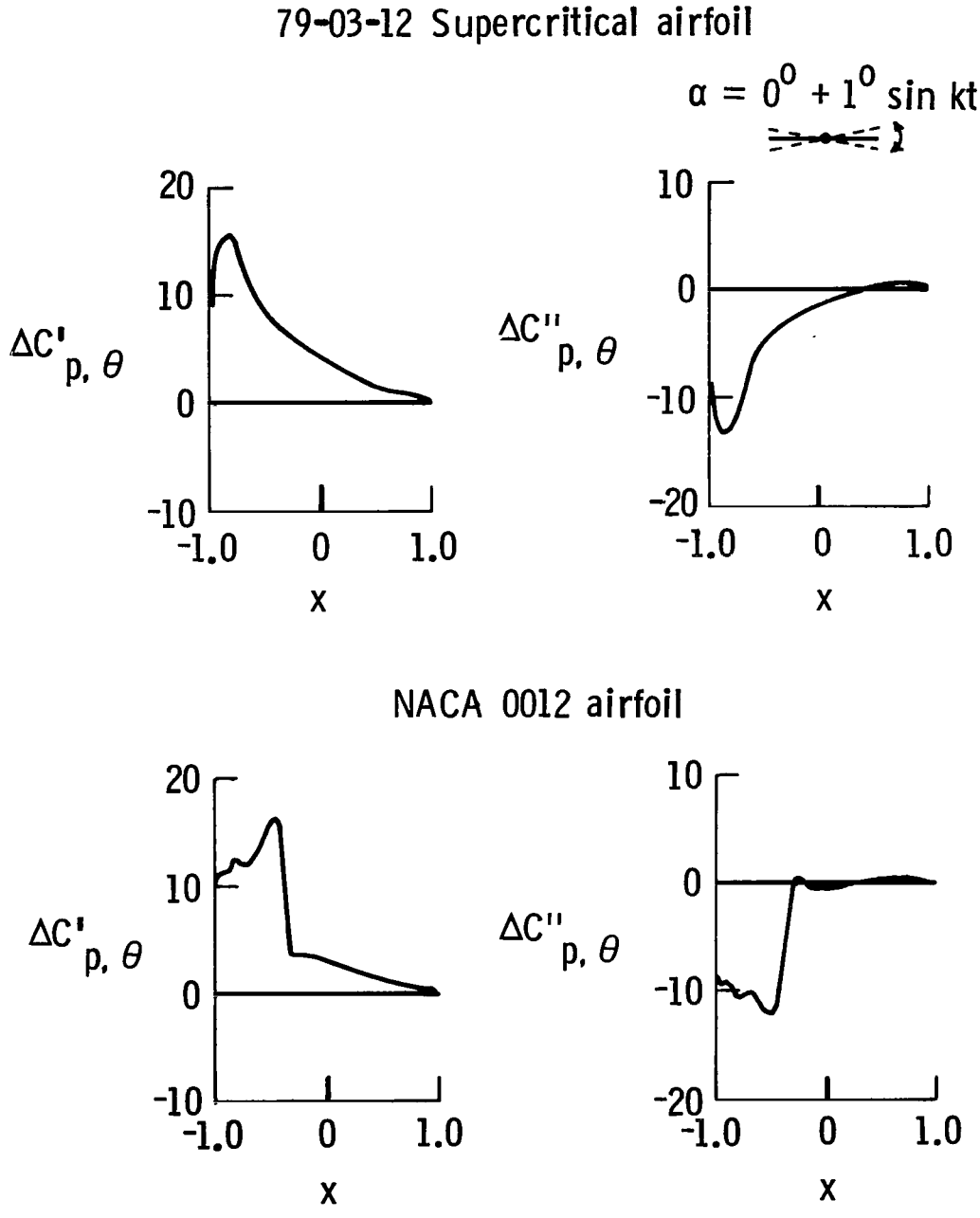

(b) $M_\infty = 0.75$; $k = 0.10$.

Figure 12.- Continued.

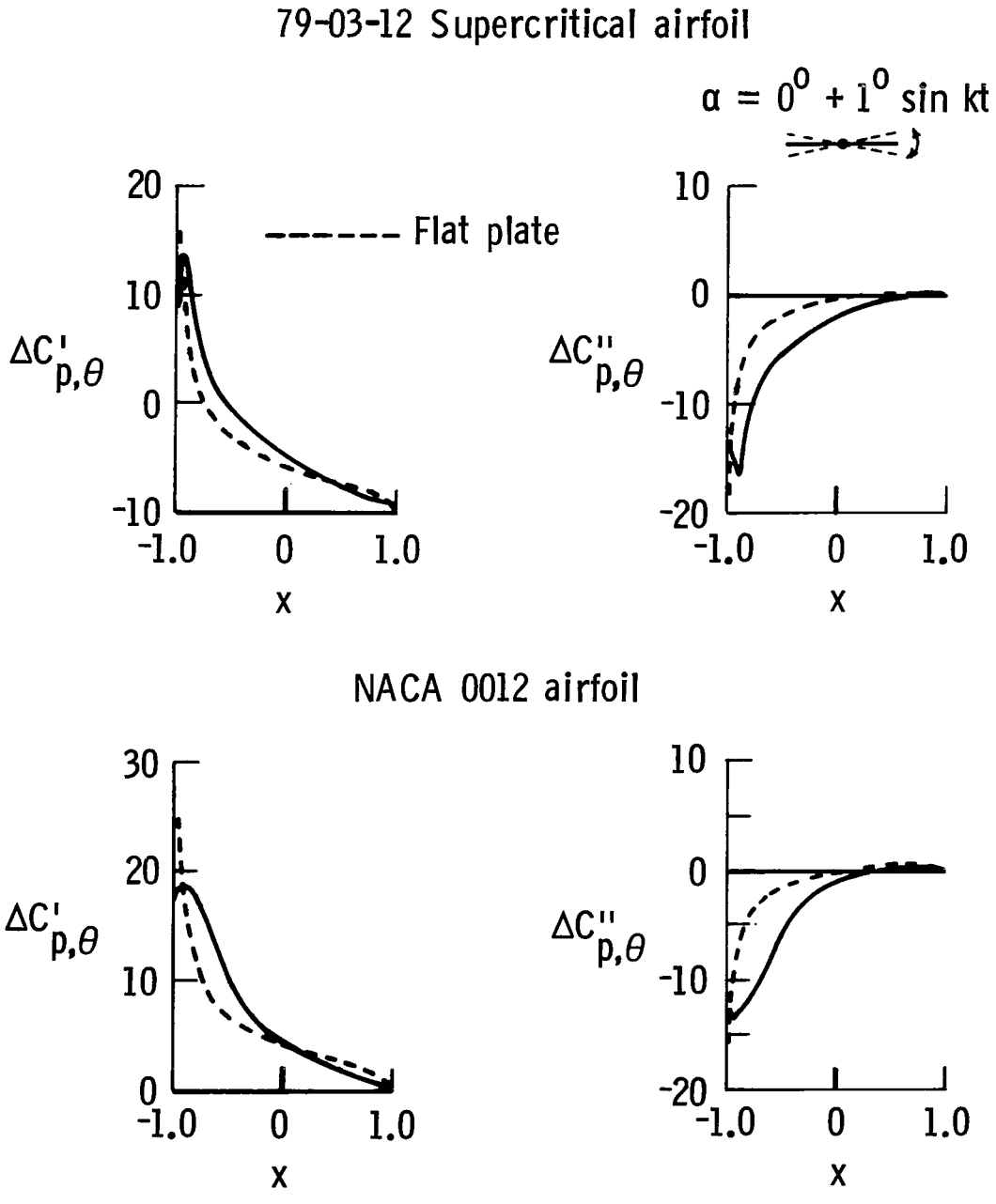

(c) $M_\infty = 0.70$; $k = 0.10$.

Figure 12.- Concluded.

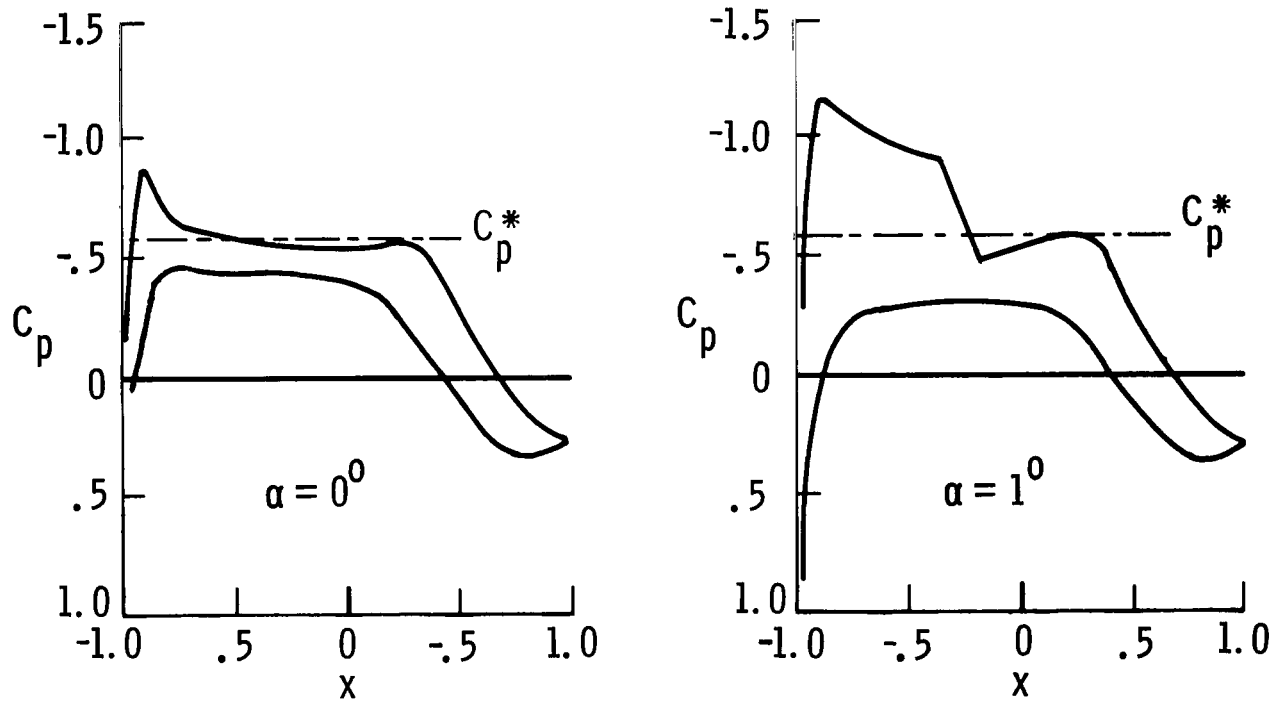

Figure 13.- Steady pressure distributions on 79-03-12 supercritical airfoil at $M_\infty = 0.75$.

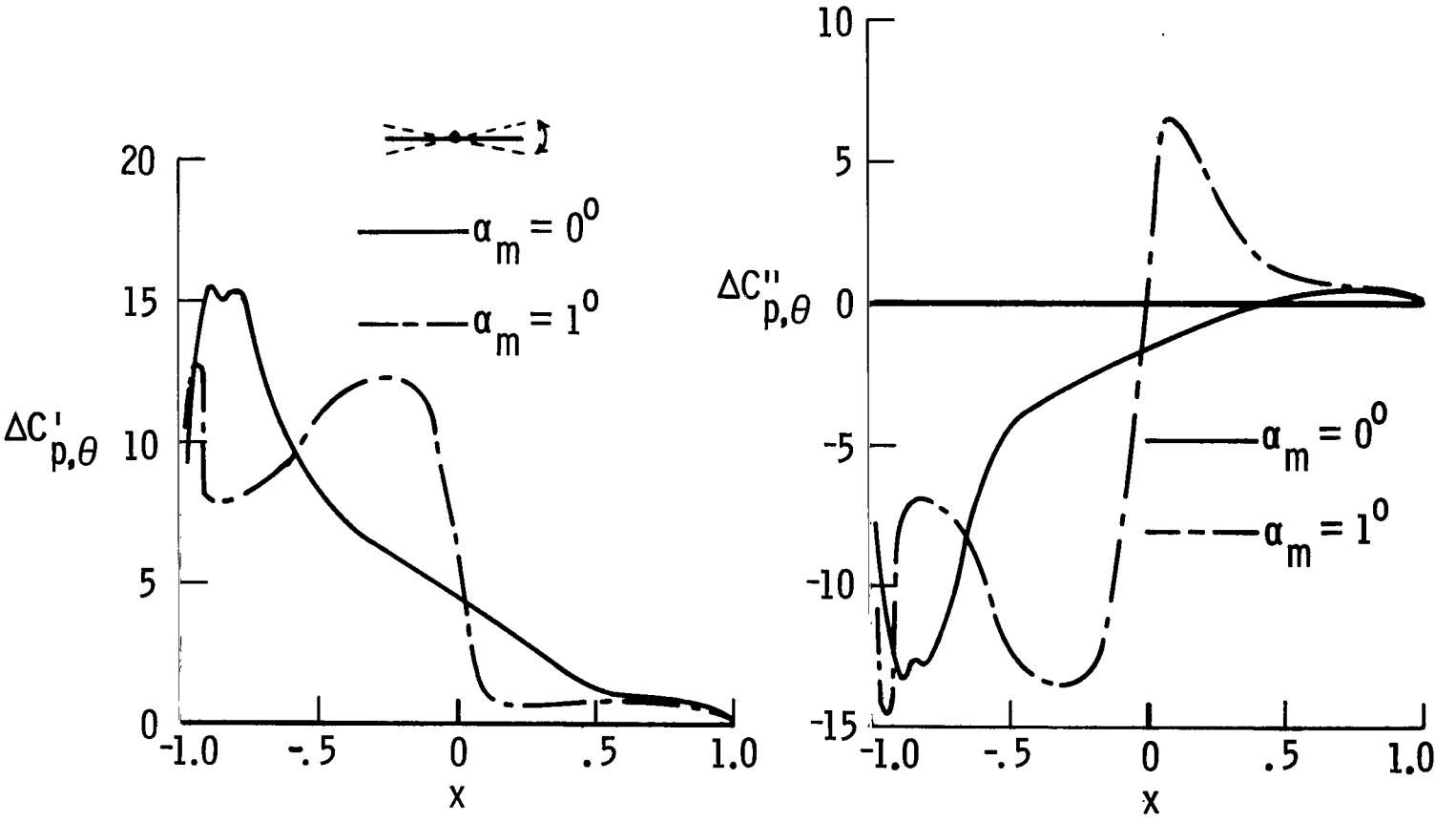

Figure 14.- The effect of mean angle of attack on unsteady load distribution on 79-03-12 supercritical airfoil oscillating in pitch about midchord axis. $M_\infty = 0.75$; $k = 0.10$; $\alpha = \alpha_m + 1^o \sin kt$.

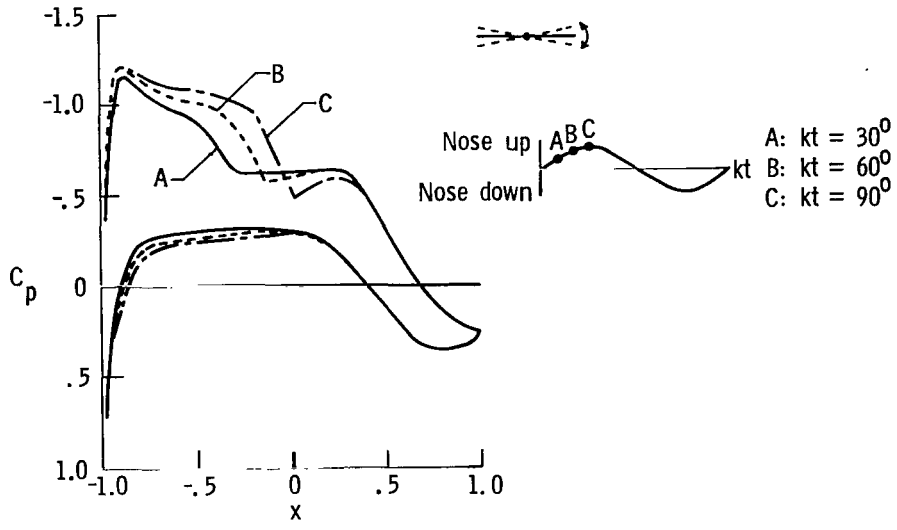

(a) kt = 30°, 60°, 90°.

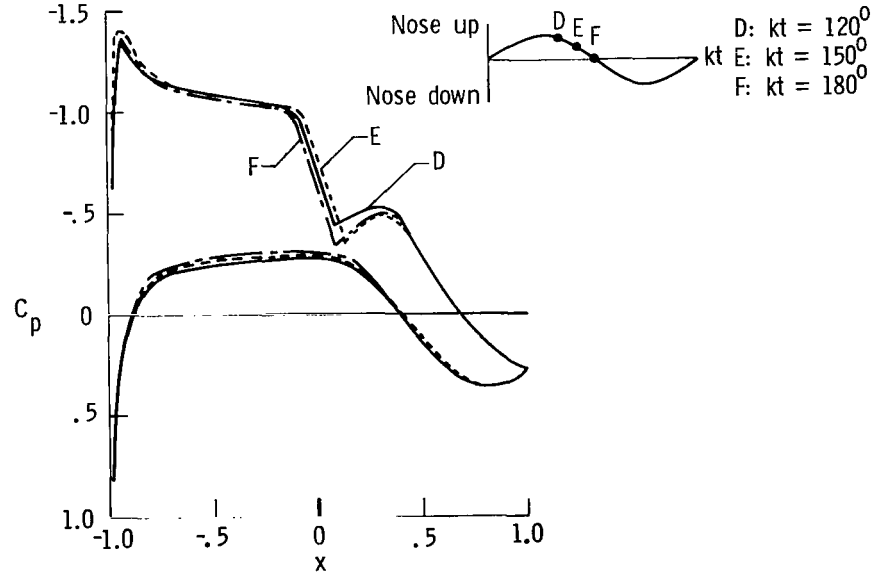

(b) kt = 120°, 150°, 180°.

Figure 15.- Unsteady pressure distribution on 79-03-12 supercritical airfoil oscillating in pitch about midchord axis at $M_\infty = 0.75$ and $k = 0.10$; $\alpha = 1^\circ + 1^\circ \sin kt$.

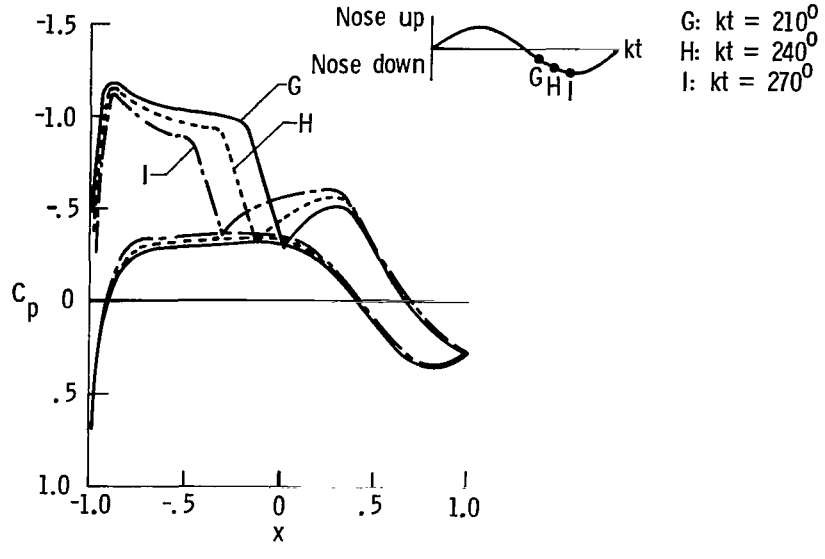

(c) kt = 210°, 240°, 270°.

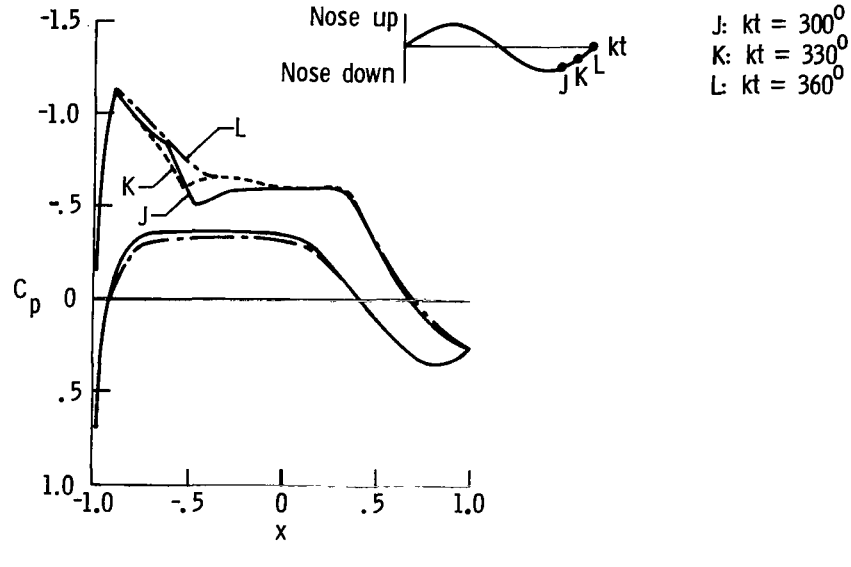

(d) kt = 300°, 330°, 360°.

Figure 15.- Concluded.

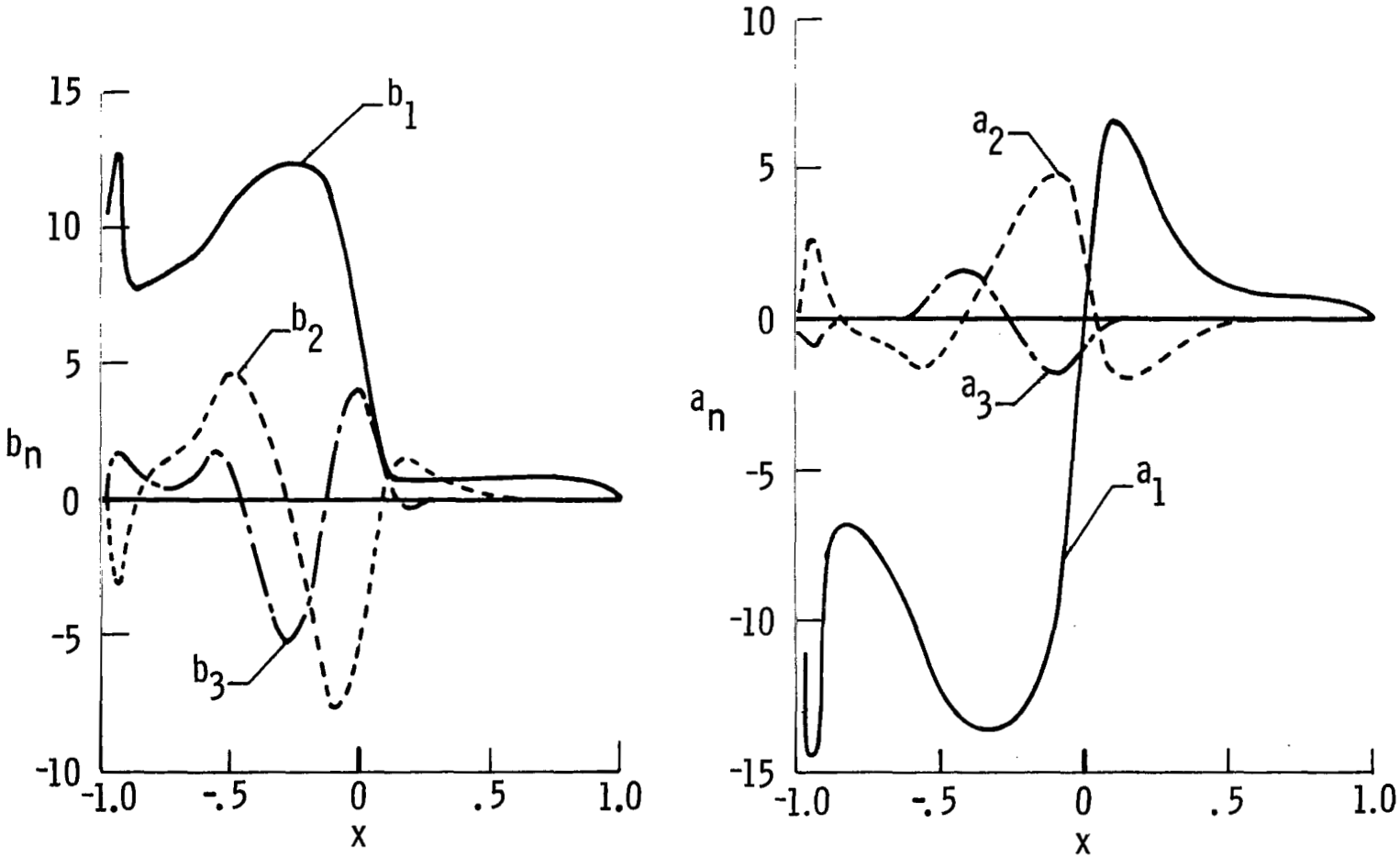

(a) b_n, n = 1, 2, 3.

(b) a_n, n = 1, 2, 3.

Figure 16.- Chordwise distributions of harmonic components of unsteady pressure loadings on 79-03-12 supercritical airfoil oscillating in pitch about mid-chord axis at $M_\infty = 0.75$ and $k = 0.10$; $\alpha = 1^o + 1^o \sin kt$.

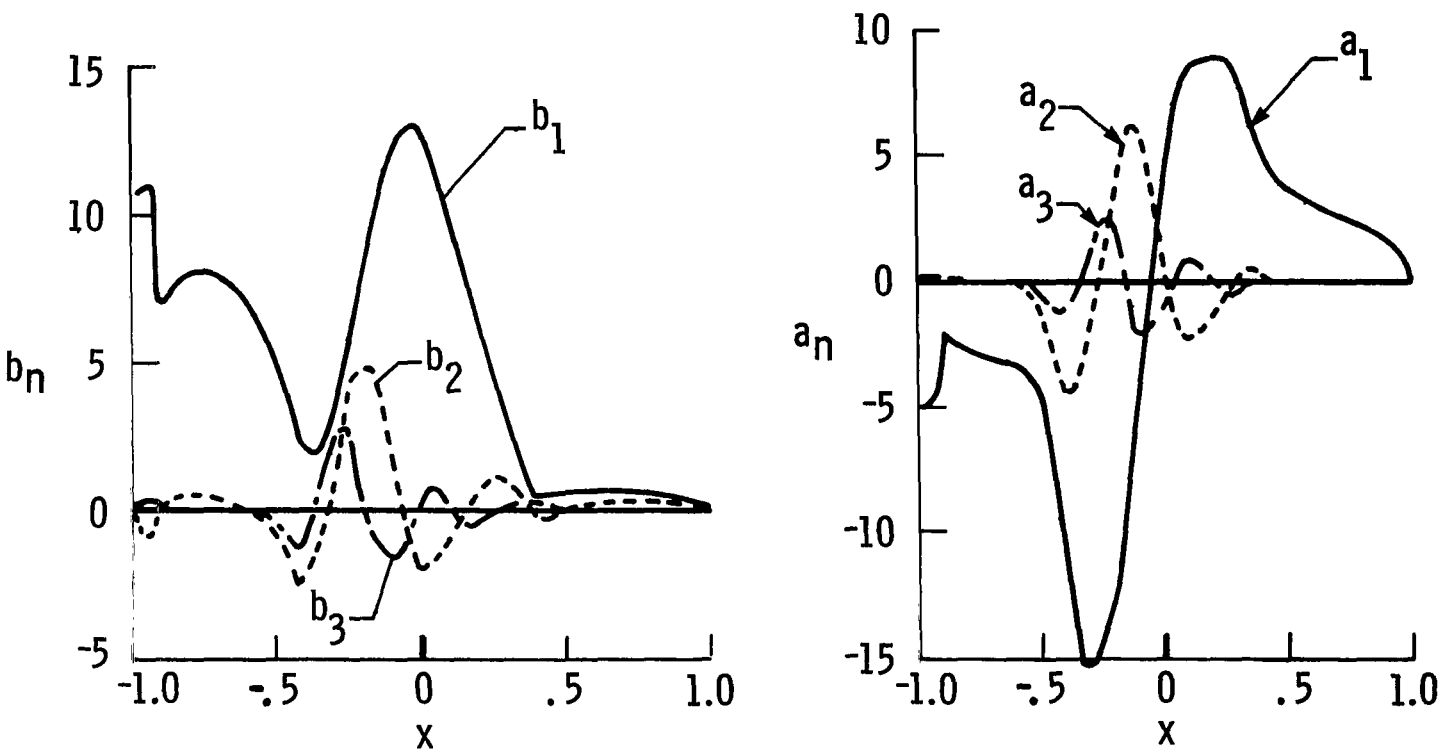

(a) b_n, n = 1, 2, 3.

(b) a_n, n = 1, 2, 3.

Figure 17.- Chordwise distribution of harmonic components of unsteady pressure loadings on 79-03-12 supercritical airfoil oscillating in pitch about mid-chord axis at $M_\infty = 0.75$ and $k = 0.30$; $\alpha = 1^o + 1^o \sin kt$.

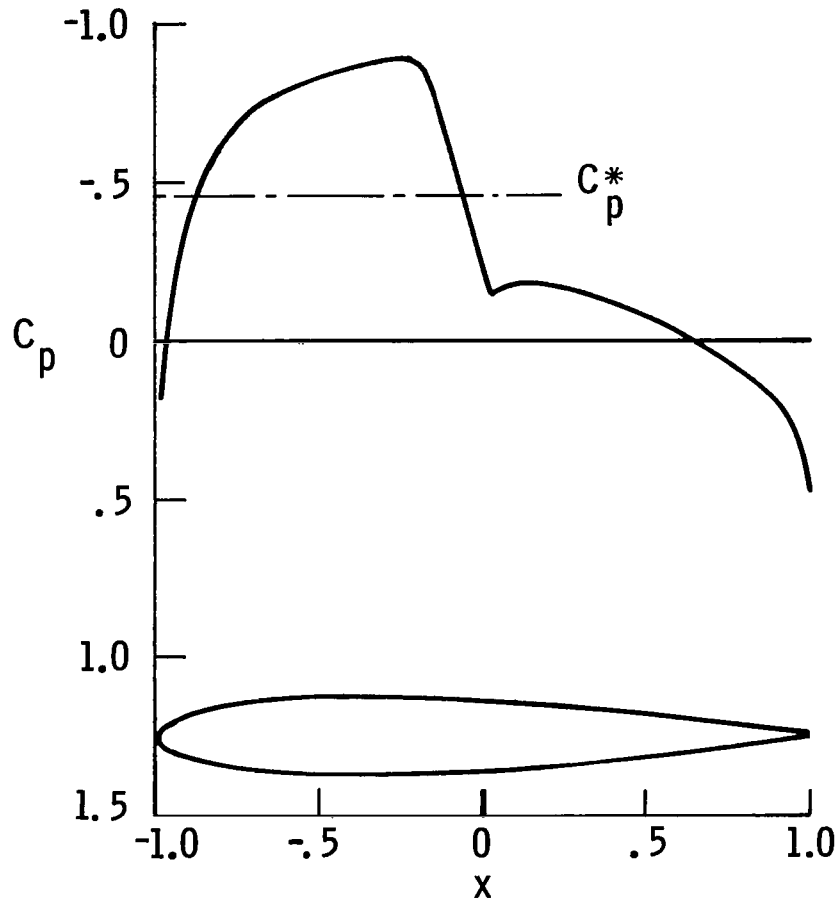

Figure 18.- Steady pressure distribution on NACA 0012 airfoil. $M_\infty = 0.79$; $\alpha = 0^o$.

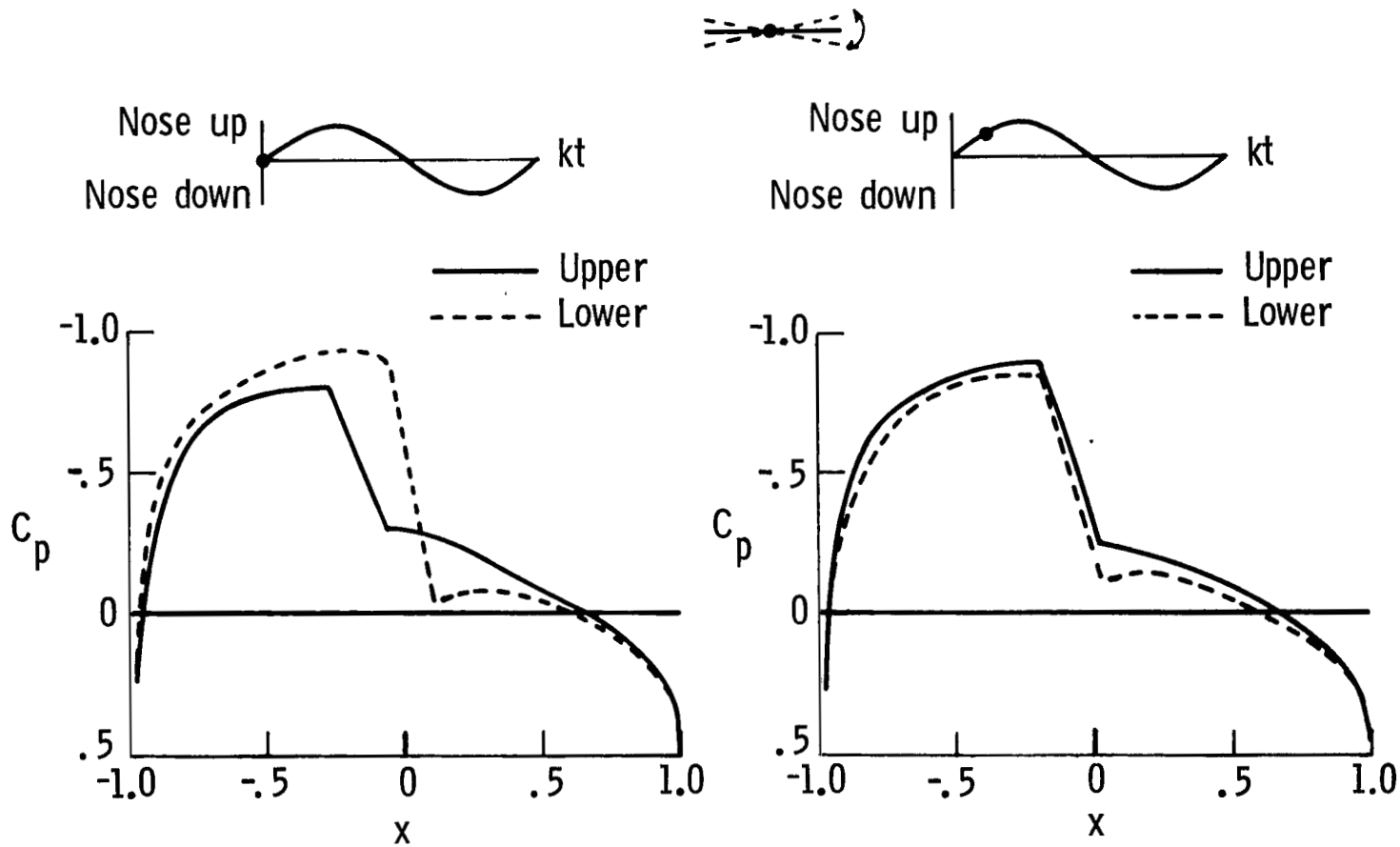

(a) kt = 0°. (b) kt = 45°.

Figure 19.- Unsteady pressure distribution on NACA 0012 oscillating in pitch about midchord axis at $M_\infty = 0.79$ and $k = 0.10$; $\alpha = 0^\circ + 1^\circ \sin kt$.

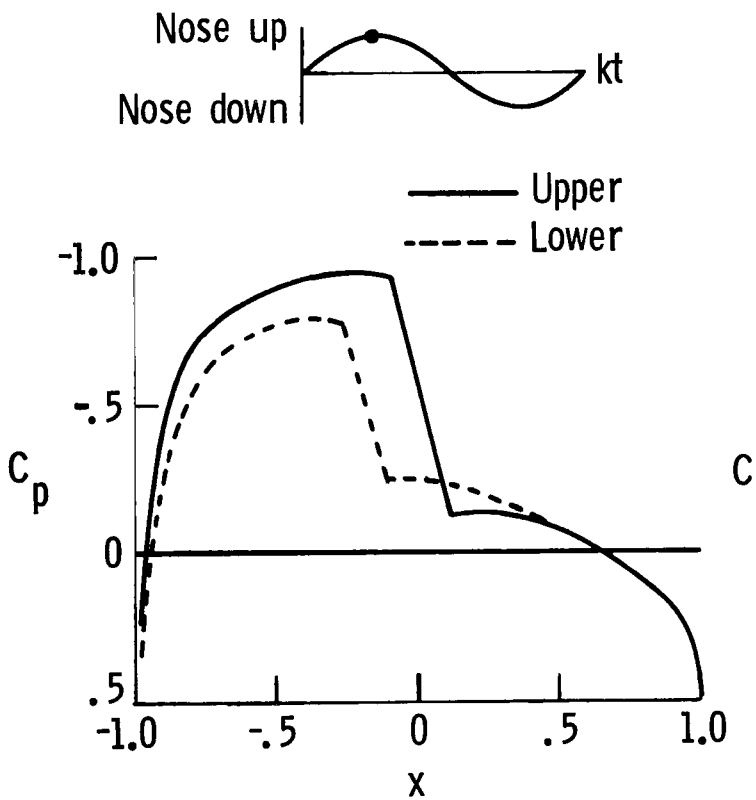

(c) kt = 90°.

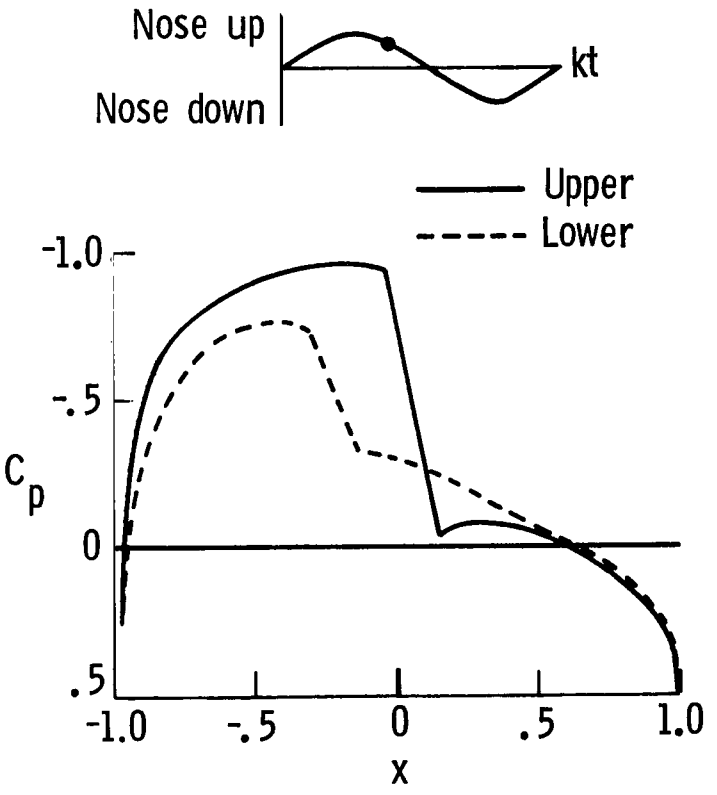

(d) kt = 135°.

Figure 19.- Concluded.

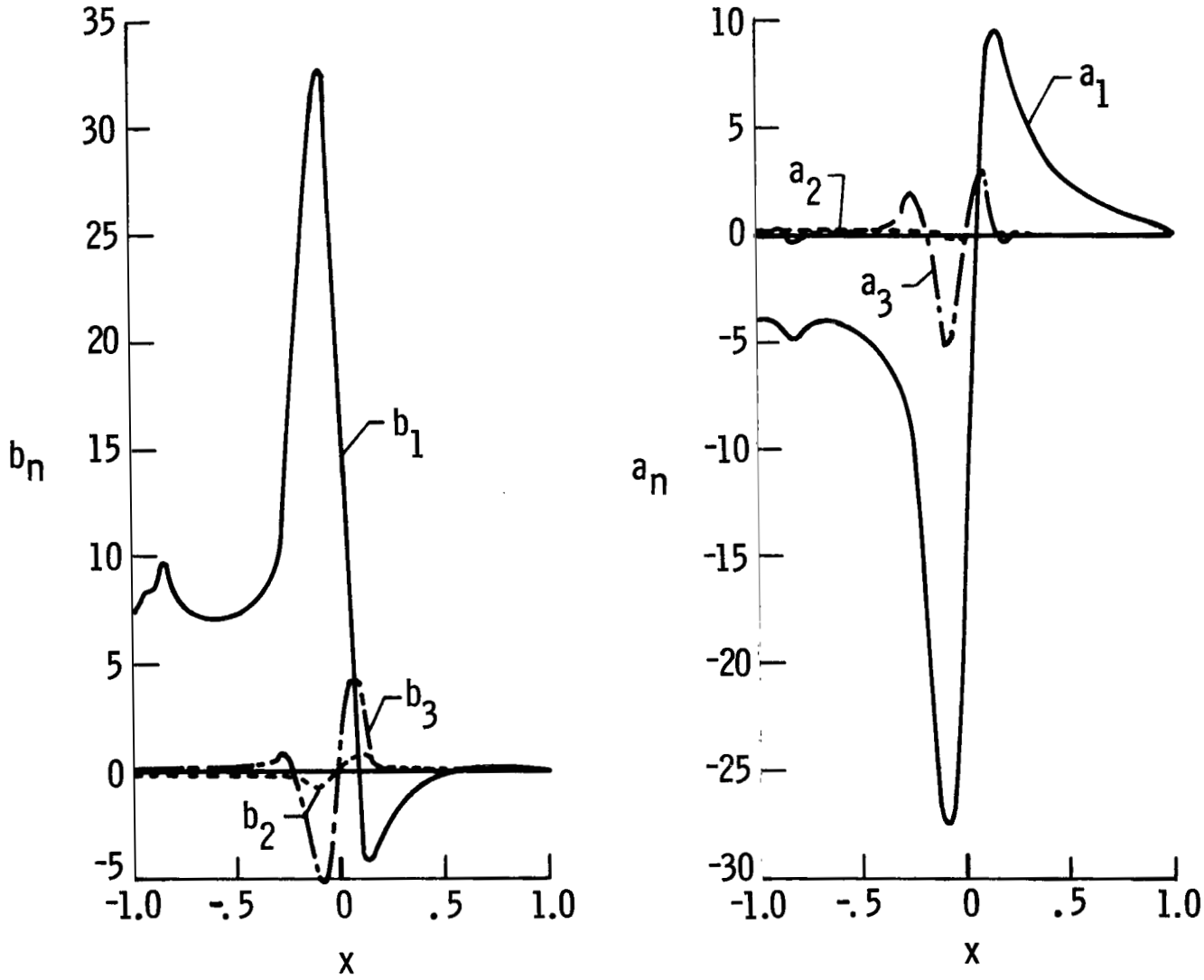

(a) b_n, n = 1, 2, 3.

(b) a_n, n = 1, 2, 3.

Figure 20.- Chordwise distribution of harmonic components of unsteady pressure loadings on NACA 0012 airfoil oscillating in pitch about midchord axis at $M_\infty = 0.79$ and $k = 0.10$; $\alpha = 0^o + 1^o \sin kt$.

1. Report No.	2. Government Accession No.	3. Recipient's Catalog No.
NASA TP-1120		

4. Title and Subtitle	5. Report Date
NUMERICAL STUDY OF TRANSONIC FLOW OVER OSCILLATING AIRFOILS USING THE FULL POTENTIAL EQUATION	April 1978
	6. Performing Organization Code
7. Author(s)	8. Performing Organization Report No.
Koji Isogai	L-11984
	10. Work Unit No.
9. Performing Organization Name and Address	505-02-21-01
NASA Langley Research Center Hampton, VA 23665	11. Contract or Grant No.
	13. Type of Report and Period Covered
12. Sponsoring Agency Name and Address	Technical Paper
National Aeronautics and Space Administration Washington, DC 20546	14. Sponsoring Agency Code

15. Supplementary Notes

Koji Isogai: NRC-NASA Resident Research Associate, on leave from National Aerospace Laboratory, Tokyo, Japan.

16. Abstract

The behavior of unsteady aerodynamic loadings on airfoils oscillating in transonic flow has been investigated numerically with particular attention given to supercritical airfoil sections. A previously developed finite difference method, which is based on the full potential equation and which uses a quasi-conservative scheme for proper capture of a shock wave motion, was employed for the present study. The unsteady aerodynamic pressure and load distributions on several different airfoil sections are presented with particular emphasis on the effects of free-stream Mach number, reduced frequency, and mean angle of attack. These parameters are demonstrated to have a significant effect on the behavior of the unsteady aerodynamic loadings. Comparisons of the present calculations with the exact inviscid solution and with the experimental results are also presented.

17. Key Words (Suggested by Author(s))	18. Distribution Statement
Two-dimensional transonic flow Unsteady aerodynamics Finite difference analysis Oscillating airfoils	Unclassified - Unlimited Subject Category 02

19. Security Classif. (of this report)	20. Security Classif. (of this page)	21. No. of Pages	22. Price*
Unclassified	Unclassified	38	$4.50

* For sale by the National Technical Information Service, Springfield, Virginia 22161

NASA-Langley, 1978

2 1 1U,A, 040878 S00903DS
DEPT OF THE AIR FORCE
AF WEAPONS LABORATORY
ATTN: TECHNICAL LIBRARY (SUL)
KIRTLAND AFB NM 87117